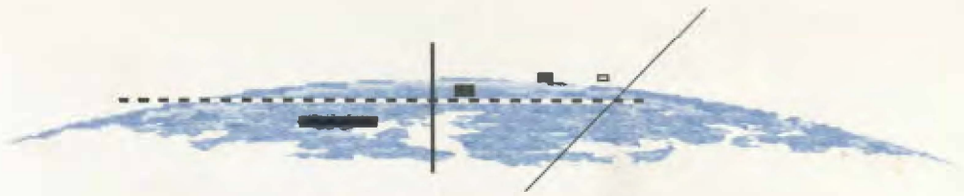

GeoForschungsZentrum Potsdam
STIFTUNG DES ÖFFENTLICHEN RECHTS

Michael Berger,
Hermann Kaufmann, Yan Ziman,
Alexej Kuzmin, Andrej Nikitin,
Ivan Polyanski, Alexander Vasileiski,
Dieter Oertel, Boris Zhukov

Entwicklung neuer Bildregistrierungsverfahren zur Fusion von Fernerkundungsdatensätzen mit unterschiedlichen geometrischen und spektralen Auflösungen

Scientific Technical Report STR98/02

Impressum

GeoForschungsZentrum Potsdam
Telegrafenberg
D-14473 Potsdam

e-mail: postmaster@gfz-potsdam.de
www: http://www.gfz-potsdam.de

Gedruckt in Potsdam
März 1998

Michael Berger,
Hermann Kaufmann, Yan Ziman,
Alexej Kuzmin, Andrej Nikitin,
Ivan Polyanski, Alexander Vasileiski,
Dieter Oertel, Boris Zhukov

Entwicklung neuer Bildregistrierungsverfahren zur Fusion von Fernerkundungsdatensätzen mit unterschiedlichen geometrischen und spektralen Auflösungen

---

Endbericht
zum Vorhaben BMBF 93F20GUS

Scientific Technical Report STR98/02

Inhaltsverzeichnis

Zusammenfassung

Ziel des Vorhabens war es, neue, voll- bzw. halbautomatische Verfahren für die geometrische Bildregistrierung von Fernerkundungsdatensätzen mit unterschiedlichen geometrischen und spektralen Auflösungen zu entwickeln und anhand von exemplarischen Beispielen zu verifizieren.

Die geometrische Bildregistrierung ist für viele Bildverarbeitungsmethoden eine notwendige Vorverarbeitung. So lassen sich Datensätze von mehreren Aufnahmezeitpunkten erst nach einer Ko-registrierung bzgl. der Veränderungsdynamik analysieren. Insbesondere Bildverarbeitungsverfahren zur Überlagerung von Datensätzen mit unterschiedlichen spektralen und geometrischen Auflösungen erfordern eine genaue Ko-registrierung.
Im allgemeinen wird die geometrische Bildregistrierung manuell durch die Detektion und Zuweisung von identischen Punkten in den zu registrierenden Bildpaaren durchgeführt. Je nach Bildinhalt kann die manuelle Zuweisung der Paßpunkte ungenau und zeitintensiv sein. Die Entwicklung von halb- bzw. vollautomatischen Bildregistrierungsverfahren ist deshalb Gegenstand intensiver Forschungsarbeiten.
Die automatische Paßpunktbestimmung stellt ein komplexes Problem dar, das sich nicht für alle Applikationen befriedigend genau mit nur einem allgemeingültigen Verfahren lösen läßt. Es hat sich gezeigt, daß Kombinationen aus verschiedenen Lösungsansätzen am effizientesten sind.

Im Rahmen des Projektes konnten zwei neue Verfahren zur automatischen Paßpunktbestimmung vorgestellt werden. Hierbei handelt es sich um ein flächenbasiertes und um ein merkmalsbasiertes Verfahren. Beide Verfahren wurden inszwischen auf internationalen Fachtagungen vorgestellt und diskutiert.

Das flächenbasierte Verfahren beruht auf einem iterativen Prozeß, bei dem die Genauigkeit mit der Anzahl der Iterationen zunimmt. Zuerst werden die Bilder in Blöcke gleicher Größe eingeteilt und nach ihren Entropiewerten sortiert. Mit Hilfe einer Korrelationsanalyse im Frequenzraum werden ähnliche Blöcke einander zugewiesen. Durch Iteration des Prozesses, wobei die Blockgröße sukzessiv verkleinert wird, werden Paßpunkte mit einer Genauigkeit kleiner als ein Pixel lokalisiert. Erste Ergebnisse an realen Fernerkundungsdatensätzen sind vielversprechend. Bislang ist das Verfahren nur für Datensätze geeignet, die annähernd im gleichen Maßstab vorliegen und die nicht mehr als 8° gegeneinander rotiert sind. In weiterführenden Arbeiten soll das Programm mit Hilfe von neuen Vergleichsalgorithmen für beliebige Rotationswinkel und Maßstäbe ausgebaut werden.

Das merkmalsbasierte Verfahren verwendet Kreuzungspunkte geradliniger Bildstrukturen zur automatischen Paßpunktbestimmung. Diese werden mit Hilfe der Hough Transformation mathematisch beschrieben. Es hat sich gezeigt, daß die Verwendung von Bildlinearen zur automatischen Paßpunktbestimmung vor allem zur Ko-registrierung von Bilddaten, die in unterschiedlichen Spektralbändern aufgezeichnet wurden, geeignet sind. Dies ist dadurch begründet, daß sich viele lineare Strukturen in verschiedenen Bändern durchpausen. Ein weitere Vorteil des Verfahrens liegt in der Robustheit gegenüber Bildrauschanteilen. In weiterführenden Arbeiten sollen Untersuchungen zu unterschiedlichen Sonnenazimuth- und ele-

vationswinkeln während der Datenaufzeichnung vorgenommen und als Korrekturteil mit einbezogen werden. Zudem hat sich die gewählte Blockgröße sensitiv für die Genauigkeit gezeigt. Hierfür sind ebenfalls weiterführende Untersuchungen notwendig.

Beide Verfahren wurden mit Hilfe der IDL Entwicklungsumgebung in eine nutzerfreundliche Oberfläche programmiert und auf verschiedenen Plattformen implementiert. Die entwickelten Methoden wurden anhand von realen Fernerkundungsdatensätzen verifiziert und belegen den Zeit- und Genauigkeitsgewinn insbesondere des flächenbasierten Verfahrens im Vergleich zur manuellen Paßpunktbestimmung.

Verwendung der Zuwendungsmittel

Das Projekt wurde zu 100% vom BMBF (Kennzeichen 03F20GUS) gefördert. In der Vorkalkulation waren FE-Fremdleistungen sowie Reisekosten enthalten.

Die FE Fremdleistungen wurden gemäß der Vorkalkulation verwendet und gliedern sich in Sachmittel (Bildverarbeitungsworkstation incl. Bildverarbeitungssoftware und Entwicklungssoftware) sowie in Personalkosten zur Unterstützung des russischen Partners.

Durch die Zuwendungsmittel konnten dem Space Research Institute (IKI) der russischen Akademie der Wissenschaften zwei leistungsfähige Bildverarbeitungsworkstationen (SGI) incl. Bildverarbeitungssoftware (ENVI) und Entwicklungssoftware (IDL) übergeben werden. Der Preisverfall auf dem IT Sektor ermöglichte es, anstatt der ursprünglich geplante SUN ULTRA Workstation, zwei SGI Workstationen mit höherer Rechenleistung bei gleichen Investitionskosten, anzuschaffen. Dies erschien sinnvoll, da mehrere Wissenschaftler am IKI gleichzeitig mit Aufgaben des Vorhabens betraut waren.
Durch die Übergabe der Bildverarbeitungsstationen wurde es dem IKI ermöglicht, Anschluß in der Bildverarbeitungsforschung zu halten.

Neben den Sachmitteln konnten für die Zeitdauer des Vorhabens insgesamt fünf Wissenschaftler am IKI finanziell unterstützt werden. Dies hat sich positiv zur Haltung der fachlichen Kompetenz ausgewirkt. Abwanderungstendenzen, insbesondere von Nachwuchswissenschaftler in fachfremde Industriezweige konnte damit entgegengewirkt werden.

Die Reisekosten wurden gemäß Vorkalkulation verwendet.

Durch die Projektreffen am IKI in Moskau konnten auftretende Kommunikationsschwierigkeiten gelöst sowie neue Kontakte geknüpft bzw. bereits existierende Kontakte intensiviert werden. Von beiden Partnern wurde bei der Projektabschlußsitzung ausdrücklich der Wunsch nach zukünftiger Zusammenarbeit geäußert.

Anstatt des ursprünglich vorgesehenen Aufenthaltes eines IKI Wissenschaftlers für zwei Monate am GFZ, wurden auf Wunsch der russischen Projektleitung, zwei Wissenschaftler für die Zeitdauer von einem Monat entsandt. Dem wurde zugestimmt, da die Softwareimplementation sowie anfälligen Verbesserungsarbeiten in diesem Zeitraum zu bewältigen waren. Dadurch wurde es zwei jungen russischen Wissenschaftlern ermöglicht, einen Einblick in die Arbeitsweise einer deutschen Großforschungsanstalt zu gewinnen.

Sonstige Reisekosten wurden für internationale Tagungen verwandt, auf denen die neuentwickelten Methoden vorgestellt und diskutiert wurden. Neben dem wichtigen wissenschaftlichen Austausch, konnten Kontakte zu länderübergreifenden Organisationen (z.B. EARSeL - Data Fusion Committee) geknüpft werden.

1. Einleitung

Daten von flugzeug- und satellitengetragenen Fernerkundungssystemen werden in vielfältiger Weise zur Charakterisierung der Erdoberfläche bzw. zur Erforschung der Phänomene, die zu ihrer Veränderung beitragen, eingesetzt. Hierbei werden von unterschiedlichen Systemen, je nach ihrer spektralen Auslegung und ihrer geometrischen Auflösung, unterschiedliche Oberflächenphänomene erfaßt. Digital aufbereitete thematische Informationen aus anderen Quellen können zudem zur Unterstützung der Studien beitragen.

Um den unterschiedlichen Informationsgehalt der Daten synergetisch in Bildanalyseverfahren bzw. in Geographischen Informationssystemen auswerten zu können, müssen die Daten aus unterschiedlichen Quellen geometrisch überlagert vorliegen. Hierzu werden Bildregistrierungsverfahren eingesetzt.

Die geometrische Bildregistrierung ist für viele Bildverarbeitungsmethoden eine notwendige Vorverarbeitung. So lassen sich Datensätze von mehreren Aufnahmezeitpunkten (multitemporal) erst nach einer Ko-registrierung bzgl. der Veränderungsdynamik (change detection) analysieren. Insbesondere Bildverarbeitungsverfahren zur Überlagerung von Datensätzen mit unterschiedlichen spektralen und geometrischen Auflösungen (meist multi-sensorale Datensätze) erfordern eine genaue Ko-registrierung. So wird z.B. die hohe räumliche Auflösung des panchromatischen SPOT HRV Kanals mit den weniger gut räumlich, aber wesentlich höher spektral auflösenden LANDSAT TM Daten, nach einer Ko-registrierung und mit Hilfe der Datenfusion überlagert. Die fusionierten Daten geben sowohl die Textur als auch die spektrale Charakteristik der Oberfläche gemeinsam wieder und können wesentlich zum Informationsgewinn beitragen.

Eine geometrische Ko-registrierung wird in drei Arbeitsschritten durchgeführt. Zuerst werden identische Punkte (Paßpunkte) im zu registrierenden Bild (Target) und im Referenzbild, welches i. allg. bereits mit Hilfe einer Karte in eine bestimmte Projektion gebracht wurde, zugewiesen. Anhand der Paßpunkte wird eine Transformation gemäß einer vorgegebenen Abbildungsvorschrift (affin bzw. polynomial) berechnet und anschließend das Targetbild mit Hilfe der Transformation entzerrt. Die Zuweisung der Paßpunkte kann manuell bzw. automatisch geschehen. Eine manuelle Zuweisung kann mit einer relativ hohen Genauigkeit für Daten, die unter ähnlichen Bedingungen aufgezeichnet wurden (gleiches Aufnahmesystem, ähnliche geometrische Auflösung, ähnliche spektrale Auflösung, ähnliche Beleuchtungsbedingungen, gleiche Jahreszeit), durchgeführt werden. Hierbei werden vom Operator in den zu registrierenden Bildpaaren identische Objekte (z.B. Straßenkreuzungen) zugewiesen.

Die manuelle Identifikation geeigneter Paßpunkte kann je nach Bildinhalt ungenau und zeitintensiv sein. Zur Überlagerung von multi-sensoralen und multi-temporalen Datensätzen, d.h. von Datensätze, die unterschiedliche Bildinformationen wiedergeben, werden deshalb halb- bzw. vollautomatische Bildregistrierungsverfahren gefordert. Sie sind seit einiger Zeit Gegenstand intensiver Forschungsarbeiten.

2. Zielsetzung und Arbeitsplan

Ziel des Vorhabens war es, neue, voll- bzw. halbautomatische Verfahren für die geometrische Bildregistrierung von Fernerkundungsdatensätzen mit unterschiedlichen geometrischen und spektralen Auflösungen zu entwickeln und diese anhand von exemplarischen Beispielen zu verifizieren.

Zum Erreichen der Zielsetzung wurde das Vorhaben in 3 Phasen durchgeführt. Im einzelnen lassen sich die Projektpasen wie folgt beschreiben:

Phase I: *Definitionsphase: Nov. – Dec. '96*
Treffen aller Projektbeteiligten, Installation der Hard- und Entwicklungssoftware, Ausarbeitung eines detaillierten Arbeitsplanes

Phase II: *Entwicklungsphase: Jan. – Aug. '97*
Entwicklung der Verfahren, Überprüfung der Verfahren, Verbesserungen, Softwareimplementation auf verschiedenen Plattformen

Phase III: *Verifikationsphase: Aug. – Dec. '97*
Durchführung und Überprüfung der Verfahren anhand von exemplarischen Anwendungsbeispielen, Anfertigung des Endberichts

Das Projekt 'Kick-Off-Meeting' fand vom 15. – 16.12.1996 am IKI in Moskau statt. Folgendes Arbeitsprogramm wurde definiert:

- Recherche des Status Quo's in der Entwicklung von neuen Verfahren zur automatischen Paßpunktbestimmung
- darauf aufbauend, die Entwicklung von neuen Verfahren,
- Umsetzung der neuen Verfahren in Softwarepakete und deren Implemenation auf verschiedenen Plattformen,
- Verifikation der neuen Verfahren anhand von realen Fernerkundungsdatensätzen.

Bei der Entwicklung und Verifikation der neuen Verfahren sollten insbesondere folgende Fälle berücksichtigt werden:

- Bildregistrierung von Datensätzen mit unterschiedlichen geometrischen Auflösungen, aber in spektral-ähnlichen Bändern,
- Bildregistrierung von Datensätzen in unterschiedlichen spektralen Bändern, wie
  - Multispektralbänder mit höher auflösenden panchromatischen Bänder,
  - Thermalkanäle mit höher auflösenden Multispektralkanälen im VIS/NIR
  - Daten von abbildenden Spektrometern mit Multispektralbänder

3. Stand der Wissenschaft

Es existiert eine Anzahl verschiedener automatischer Bildregistrierungmethoden, die je nach Aufgabenstellung und Anwendung, Vor- bzw. Nachteile aufweisen. Generell werden die Verfahren anhand der unterschiedlichen Methoden für die Paßpunktidentifikation in folgende drei Klassen eingeteilt (Cideciyan A.V. et al., 1992, Barnea and Silverman, 1972):

- manuelle Paßpunktbestimmung,
- automatische, flächenbasierte Paßpunktbestimmung (area-based),
- automatische, merkmalsbasierte Paßpunktbestimmung (feature-based)

Im einzelnen werden die automatischen Verfahren kurz erläutert.

3.1 Flächenbasierte Paßpunktbestimmung

Die flächenbasierte Paßpunktbestimmung beruht auf Ähnlichkeitsuntersuchungen der Intensitätsverhältnisse (Grauwerte) innerhalb kleiner Teilbereiche (Subsets) der zu registrierenden Bildpaare. Als Maß für die Ähnlichkeiten kommen die normalisierte Kreuzkorrelation, Korrelationskoeffizienten oder ein sequentieller Ähnlichkeitsnachweis (sequential similarity detection) zur Anwendung. D.h. ein selektiertes Subset des Referenzbildes wird statistisch mit jedem Subset des Targetbildes verglichen. Die Größe der Subsets des Referenzbildes und des Targetbildes sind dabei identisch zu wählen. Das Subset, das die höchste Korrelation aufweist, wird als identisches Subset angenommen. Bei hinreichend kleiner Subsetgröße kann der zentrale Bildpunkt als Paßpunkt zugewiesen werden.
Der Korrelationskoeffizient als Maß für die Ähnlichkeit zweier Subsets ist wie folgt gegeben:

$$C(i,j) = \frac{\sum_l \sum_m (W_z(l,m) - d_w) * (S_{ij}(l,m) - d_s)}{\sqrt{\sum_l \sum_m (W_z(l,m) - d_w)^2} * \sqrt{\sum_l \sum_m (S_{ij}(l,m) - d_s)}}$$

d_w, d_s geben die Mittelwerte der Grauwerte innerhalb des Referenzsubsets (W_z) und der Targetsubsets (S_{ij}) wieder. Die Korrelation kann im Frequenz- bzw. im Ortsraum berechnet werden. Die Berechnung des Korrelationskoeffizienten im Ortsraum ist vor allem für Bildpaare, die vom gleichen Sensor oder zumindest von Sensoren mit ähnlichen geometrischen Auflösungen aufgezeichnet wurden, geeignet (Hanizumi und Fajimura, 1993). Die Korrelation im Frequenzraum (Fourier- (Barnea und Silverman, 1972) bzw. Wavelet-Transformation (Li et al., 1995)) wird vor allem für Bildpaare, die von Sensoren mit unterschiedlicher 'inneren' und 'äußeren' Geometrie aufgezeichnet wurden, angewendet. Um die Rotation der Translation zu entkoppeln, wird das Amplitudenspektrum der Fouriertransformierten benutzt (Hanizumi und Fajimura, 1993). Datensätzen, die eine relativ große Rotation zueinander aufweisen, werden zunächst mit Hilfe der 'illuminate direction estimation' Methode bzgl. der Rotation korrigiert. Anschließend werden die Paßpunkte im Ortsraum mit Hilfe von Korrelationsverfahren bestimmt (Le Moigne, 1994).

Neben den Korrelationsmethoden kommt auch der sequentielle Ähnlichkeitsnachweis (sequential similarity detection (Goshtasby and Stockman, 1985)) als Maß zur Anwendung. Er ist wie folgt gegeben,

$$E(i,j) = \sum_{l}\sum_{m} | W(l,m) - S_{ij}(l,m)$$

Er basiert auf der Analyse von Grauwertdifferenzen des Referenzsubsets zu den Tragetsubsets. Das Maß E(i,j) wird akkumulativ für alle Pixel des Subsets berechnet bis ein vorgegebener Schwellwert überschritten wird. Die Anzahl der Pixel bis zum Erreichen des Schwellwertes wird gespeichert und als Maß für die Zuweisung identischer Subsets benutzt. Gegenüber den Korrelationsverfahren benötigt der sequentelle Ähnlichkeitsnachweis weniger Rechenleistung.

Zum Abschluß des Kapitels sind in Tabelle 1 gängige Methoden, die auf einer flächenbasierten Paßpunktbestimmung beruhen, vergleichend gegenübergestellt.

Tabelle 1: *Gegenüberstellung flächenbasierter Verfahren zur Paßpunktbestimmung*

Ref.	Sensor	Image Overlap	Feature & Feature Matching	Transformation	Advantages and Limitation
Hanizumi und Fajimura, 1993	single, visual camera	large	area-based, cross-correlation	affine (RTS)	good performance on noisy image, region of interest must be visible completely in both images
Li et al., 1995	single, SAR images	large	area-based, analysis in the Fourier domain and Cepstrum domain	affine (RT)	region of interest must be visible completely in both images, noise-tolerant and computationally efficient
Barnea und Silverman , 1972	single, visual camera, Landsat TM	large	combined technique in transform domain, maxim of wavelet coefficients, cross-correlation, mutiresolution strategy	affine (R)	images with only rotational difference are used
Kher und Mitra, 1994	single, visual camera, optical sensor	small	combined technique, Gabor wavelet transform for feature extraction plus correlation in spatial domain	affine (RTS)	tolerate large rotation and translation

3.2 Merkmalsbasierte Paßpunktbestimmung

Die merkmalsbasierte Paßpunktbestimmung beruht auf der Identifikation von Bildobjekten sowie einer mathematischen Beschreibung ihrer Eigenschaften (Attributzuweisung). Hierzu werden vor allem Bildstrukturen verwendet. Die Strukturen sind durch Grauwertsprünge an Kanten unterschiedlicher Oberflächenausprägung begründet (z.B. Hausdach – Garten). Daneben lassen sich Formbeschreibungen von Flächen bzw. Texturbeschreibung für die Paßpunktzuweisung verwenden.
Die Identifikation von Paßpunkten mit Hilfe von Bildobjekten läßt sich in drei Schritte einteilen:

- zuerst werden Objekte, die untereinander gut trennbar sind, im Referenzbild identifiziert,

- anschließend werden die Objekte mathematisch beschrieben (Bildlokalisation und Attributzuweisung) und
- schließlich korrespondierende Objekte im Targetbild gesucht.

In einigen Verfahren werden Objekte im Referenzbild und Targetbild unabhängig voneinander identifiziert und anschließend mit Hilfe ihrer Eigenschaften einander zugewiesen. Andere Methoden selektieren Objekte nur im Referenzbild und suchen anschließend nach identischen Objekten im Targetbild.

Je nach Bildinhalt eignen sich folgende Objekte zur Paßpunktbestimmung:

- homogene, klar begrenzte Flächen (z.B. Felder, Seen),
- geschlossene Grenzen von homogenen Flächen,
- nicht-geschlossene Grenzen von scharfkantigen Grauwertsprüngen (z.B. Haus-Garten),
- lineare Strukturen (z.B. Straßen, geol. Strukturen),
- Kreuzungspunkte linearer Strukturen,
- sonstige bekannte punktförmige Objekte (z.B. bekannte Gebäude).

Die Objekte werden mit Hilfe von Bildvorverarbeitungsschritten extrahiert. Hierfür kommen vor allem Segmetierungsalgorithmen wie z.B. der Gradientenfilter zur Anwendung.
Über die Lokalisation der Objekte bzw. mit Hilfe ihrer Attribute werden korrespondierende Objekte zugewiesen. Im allgemeinen wird das Zentralpixel des Objekts als Paßpunkt benutzt. Es ist deshalb darauf zu achten, daß die Attribute möglichst unabhängig und robust bzgl. der Geometrie, der Radiometrie und des Rauschanteiles sind. Werden Attribute verwendet, die spektral unabhängig sind, so lassen sich Datensätze von Sensoren mit verschiedenen spektralen Bändern registrieren. Für geschlossene Grenzen (Polygone) eignen sich z.B. Formbeschreibungen wie invariante Flächenmomente als Attribute. Für nicht-geschlossenen Grenzen lassen sich Anfangs-, End-, bzw. Extremwerte verwenden. Lineare Strukturen können über Winkelanhängigkeiten sowie Distanzen charakterisiert werden, wobei die Verwendung von Kreuzungspunkten linearer Strukturen eine eindeutigere Identifizierung der Paßpunkte zulassen.
Die Zuweisung korrespondierender Objekte im Targetbild wird als eigener Arbeitsschritt der Ko-registrierung beschrieben. Es existieren Verfahren, die hierfür lediglich die relativen Koordinaten bzw. die Distanzen der Objekte im Referenz- und im Targetbild verwenden (siehe z.B. Methode nach Ranade und Rosenfeld (1980)). Nach einer Methode von Ghostaby und Stockman (1985) werden nur Objekte verwendet, die auf der Grenze eines Polygons liegen, welches alle Objekte einschließ (garbarite objects). Komplexere Methoden wie z.B. die Methode nach Wong und Hall (1978) benutzen neben den relativen Koordinaten zusätzliche Attribute (z.B. Flächenbeschreibungen) zur Objektzuweisung. Eine interessante Variante wurde von Ton und Jain (1989) vorgeschlagen. Sie verwenden einen iterativen Relaxationsalgorithmus um Objekte miteinander zu vergleichen. Die ermittelten Parameter beschreiben eine Wichtungsfunktion zur Objektzuweisung.

In Tabelle 2 sind gängige, merkmalsbasierte Bildregistrierungsmethoden gegenübergestellt.

($H(w_1)<H(w_2)....<H(w_n)$). Anschließend wird für jedes Subset des Referenzbildes das identische Subset im Targetbild gesucht.
Die Suche wird iterativ durchgeführt, wobei die Genauigkeit von Iteration zu Iteration zunimmt.
Mit Hilfe einer Korrelationsanalyse im Frequenzraum bzw. mit Hilfe der integralen Amplitudenspektren für ausgewählte Frequenzbereiche (circle frequency zone) werden zunächst mögliche Subset-Kandidaten im Targetbild identifiziert. Hierzu wird das Targetbild in gleichgroße Subsets wie das Referenzbild eingeteilt.

Die Anzahl der Subset-Kandidaten wird vom Operator vorgegeben. Die ausgewiesenen Kandidaten sowie ihrer Umgebungen werden anschließend genauer untersucht. Hierzu wird jeder Kandidat einer Intensitätskorrelationsanalyse unterzogen. Dies geschieht indem eine Korrelationsmaske pixelweise über das Kandidatensubset sowie seiner Umgebung geschoben wird. Damit läßt sich zum Referenzsubset ein Bereich im Targetbild bestimmen, der die größte Korrelation aufweist. Dieser Bereich wird als identisch zum Referenzsubset angenommen. Das zentrale Pixel wird als Paßpunkt verwendet. Die Koordinaten sind somit mit einer Genauigkeit der halben Subsetgröße bestimmt.

Die oben beschriebene Methode wird anschließend umgekehrt auf das Referenzbild angewandt. Hierzu werden die ausgewiesenen Subsets des Targetbildes fixiert, d.h. die Umgebungen der zuvor fixierten Subsets im Referenzbild werden mit Hilfe einer Korrelationanalyse untersucht und eventuell nachkorrigiert. Damit lassen sich Genauigkeiten besser als ein Pixel erreichen.

4.1.2 Zusammenfassung

Das vorgestellte, iterative Verfahren ist zur Ko-registrierung von Bilddaten geeignet, die annähernd im gleichen Maßstab vorliegen und nicht mehr als 8° gegeneinander rotiert sind. D.h. die Daten müssen bereits grob ko-registriert vorliegen. Das Verfahren ist als Feinabstimmung gedacht.
Erste Ergebnisse an realen Fernerkundungsdatensätzen sind vielversprechend, jedoch sind bereits eine Reihe von Verbesserungsvorschlägen angedacht. Insbesondere soll das Programm für beliebig Rotationswinkel und Maßstäbe ausgebaut werden. Hierzu sind neue Vergleichsalgorithmen zu entwickeln.

4.2 Paßpunktbestimmung mit Hilfe sich schneidender, linearer Bildelemente

Bei der zweiten, neu-entwickelten Methode zur automatischen Paßpunktbestimmung, handelt es sich um einen merkmalsbasierten Ansatz. Hierbei werden sich schneidende Bildlineare als Objekte verwendet. Diese sind i. allg. leicht in Fernerkundungsdatensätzen detektierbar (Grenzen zwischen verschiedenen Ackerflächen, Häusergrenzen, Straßen etc.). Von Vorteil ist, daß sich viele Bildlineare in verschiedenen Spektralbändern durchpausen. Damit ist das Verfahren gut für die Ko-registrierung von Datensätzen mit unterschiedlicher spektraler Auflösung geeignet. Wie die vorhergehende Methode, hat auch diese Methode eine 'Feinabstimmung' der Ko-registrierung zum Ziel. Deshalb ist es erforderlich, die Daten in einer Vorverarbeitung entsprechend ihrer System- und Orbitparameter zu korrigieren.

Die Methode basiert auf der Detektion und Zuweisung geradliniger Bildelemente. Das Verfahren läßt sich grob in folgende Arbeitsschritte gliedern:

- zuerst werden Grauwertgrenzen mit Hilfe von Segmentierungsalgorithmen detektiert,
- anschließend werden daraus geeignete, geradlinige Grenzen ausgewählt und diesen Attribute zugewiesen,
- die Grenzen und ihrer Attribute des Referenzbildes werden mit geradlinigen Grenzen und ihren Attributen des Targetbildes verglichen,
- und schließlich damit die Paßpunkte lokalisiert.

4.2.1 Segmentierung

Grenzen werden mit Hilfe von Segmentierungsalgorithmen ausgewiesen. So lassen sich z.B. Grauwertsprünge dadurch detektieren, indem man die Bilder mit einem Laplace-Filter filtert. Der Laplace Filter wird sowohl auf Referenz- als auch Targetbild angewandt. Anschließend werden in den Gradientenbildern nur diejenigen Pixel ausgewiesen, die einen bestimmten Grauwertsprung überschreiten. Dies geschieht mit Hilfe eines vorgegebenen Schwellwertes. Durch diese Operationen wandelt man die Grauwertbilder in Binärbilder um.

4.2.2 Selektion geeigneter Grenzen

Geeignete Grenzen werden in Referenz- und Targetbild unabhängig voneinander bestimmt. Hierzu kommt die Hough-Transformation zur Anwendung.
Zuerst werden die Binärbilder in Subsets gleicher Größe eingeteilt. Für jedes Subset wird die Hough Transformation berechnet, wodurch geradlinige Grenzen ausgewiesen werden. Anschließend wird der Einheitsvektor der Helligkeitverteilung der Hough-Transformierten in Spaltenrichtung berechnet. Er gibt ein Maß für die auftretenden Winkel und den Anteil (line power) aller geradlinigen Elemente innerhalb der Subsets wieder. Der Anteil (line power) ist durch die Anzahl der Pixel, die eine Linie bilden, gegeben. Anschließend wird ein Maß für

den Anteil der sich kreuzenden Geraden für jedes Subset berechnet. Dadurch werden Subsets ausgewiesen, die viele Kreuzungspunkte enthalten und deshalb besser zur Paßpunktbestimmung geeignet sind.

4.2.3 Zuweisung geeigneter Subsets

Geeignete Subsets, d.h. Subsets die viele Kreuzungspunkte aufweisen, werden in Referenzbild und Targetbild mit Hilfe eines Vergleichsalgorithmus sowie den relativen Positionen der Kreuzungspunkte einander zugewiesen. Für den Vergleich wird der Einheitsvektor der Helligkeitsverteilung der Houghtransformierten verwendet. Die relative Position der Kreuzungspunkte wird durch die Distanzen vom Subsetzentrum aus beschrieben. Subsets, die sich nicht eindeutig zuweisen lassen, werden automatisch ausgeschlossen.

4.2.4 Paßpunktbestimmung

Hierzu wird der Rotationswinkel und die Translation einander zugewiesener Subsets ausgewertet. Im Referenzbild wird das Zentrum des Subset als Paßpunkt, im Targetbild das Zentrumspixel verschoben um den Translationsbetrag, ausgewiesen. Dadurch läßt sich für jedes einander zugewiesene Paar von Subset ein Paßpunktpaar bestimmen. Diese werden anschließend zur Berechnung der Transformationsmatrix verwendet.

4.2.5 Zusammenfassung

Die Verwendung von Bildlinearen zur automatischen Paßpunktbestimmung ist insbesondere für die Ko-registrierung von Bilddaten, die in unterschiedlichen spektralen Bändern aufgezeichnet wurden, geeignet. Dies liegt daran, daß sich viele lineare Strukturen in verschiedenen spektralen Bändern durchpausen. Ein weiterer Vorteil ist die Robustheit des Verfahrens gegenüber Bildrauschanteilen. Geradlinige Bildelemente sind zudem leicht in Bildern zu detektieren und können mit Hilfe der Hough Transformation mathematisch beschrieben werden.
Das Verfahren wurde anhand simulierter Daten getestet. Die ersten Ergebnisse sind zufriedendstellend, jedoch sind weiterführende Arbeiten notwendig, um die Methode auszureifen. Hierbei muß das Verfahren auf Bilddaten getestet werden, die von verschiedenen Sensoren stammen und unterschiedliche Oberflächen abbilden. Zudem sind Untersuchungen zu unterschiedlichen Sonnenazimuth- und elevationswinkeln notwendig. Durch die unterschiedlichen Winkel können Bildlineare unterschiedlich ausgeprägt und verschoben sein (Schattenwurf!). Durch einen Korrekturanteil lassen sich diese Effekte bei der Paßpunktbestimmung mit berücksichtigen. Die gewählte Subsetgröße zur Beschreibung der Kreuzungspunkte hat sich als sensitiv für die erzielbare Genauigkeit gezeigt. Hierzu sind noch weiterführende Untersu-

chungen notwendig. So sind z.B. automatische Optimierungen, je nach Bildinformationsgehalt, für die Subsetgröße denkbar.

5. Literaturverzeichnis

Barnea, D.I., and Silverman, H.F., 1972, A Class of Algorithms for Fast Digital image Registration. *IEEE Trans. Comput.*, **21(2)**, 179-186.

Cheng, J.K., and Huang, T.S., Image registration by matching relational structures.- *Pattern Recog*, Vol.**17**, No 1, 149-159.

Cideciyan, A.V. & al., 1992, Registration of High-Resolution Images of the Retina. *Proceedings of the SPIE*, **59(5)**, 645-653.

Djamdji, J.-P., Bijaoui, A., and Maniere, R., 1993, Geometrical Registration of Images: The Multiresolution Approach. *PE & RS*, Vol.**59**, N5, 645-653.

Duda, R.O., and Hart, P.E., Use of the Hough Transformation to Detect Lines and Curves in Pictures.- Commun. ACM, **15, 1**, 11-15.

Flusser, J., and Suk, T., 1994, A moment based approach to registration of images with affine geometric distortion. *IEEE Trans. of Geoscience and Remote Sensing*, **32(2)**, 382-387.

Fonseca, L.M.G., and Manjunath, B.S., 1996, Registration Techniques for Multisensor Remotely Sensed Imagery. *PE & RS*, Vol. **62**, N9, 1049-1056.

Goshtasby, A., and Stockman, G.C., 1985, Point pattern matching using convex hull edges. *IEEE Trans. Syst. Man Cybernetics*, **15(5)**, 631-637.

Hanizumi, H., and Fajimura, S., 1993, An Automated Method for Registration of Satellite Remote Sensing Images. *Proceedings of IGARSS -IEEE Trans. On Geoscience and Remote Sensing Symposium*, N**3**, 1348-1350.

Hough, P.V.C., 1962, Methods and means for recognition complex patterns.- U.S.Patent 3,069, 654.

IDL Reference Guide V.2, Version 4, 1995, 1-906.

IDL User's Guide, Version 4, 1995, p.21-1.

Kher, A., and Mitra, S., 1994, Registration of noisy SAR imagery using morphological feature extractor and 2-D cepstrum. *Proc. of the SPIE*, **1771**:281-291.

Kuzmin, A., Nikitin, A., and Berger, M., 1998, Automatic Control Point Detection for Image Registration using an Iterative Approach, *Proc. of WSCG*, Prague, in print

Le Moigne, J., 1994, Parallel Registration of Multisensor Remotely Sensed Imagery Using Wavelet Coefficient. *Proceedings of SPIE*, **2242**:432-443.

Li, H., Manjunath, B.S., and Mitra, S.K., 1995, An approach to multisensor image registration. *IEEE Trans. on Image Processing*, **4(3)**:320-334.

O'Gorman, F., and Clowes, M.B., Finding picture edges through collinearity of feature points.- *IEEE Trans. Computers*, **C-25, 4**, 449-456.

Ranade, S., and Rosenfeld, A., 1980, Point pattern matching by relaxation. *Pattern Recognition*, **12**:269-275.

Ranade, S., and Rosenfeld, A., 1980, Point pattern matching by relaxation.- *Pattern Recognition*, **12**:269-275.

Renka, R., 1982, Interpolation of data on the surface of a sphere. Oak Ridge National Laboratory Report **ORNL/CSD-108**.

Rignot, E.J.M., Kowk, R., Curlander, J.C., and Pang S.S., 1991, Automated Multisensor Registration: Requirements and Techniques. *PE & RS*, vol.**57**, N8, 1029-1038.

Stockman, G.C., Kopstein, S., and Benett, S., 1982 Matching images to models for registration and object detection via clustering. *IEEE Trans. Pattern Anal. Mach. Intell.*, Vol.**PAMI-4**, 229-241.

Takeuchi, S., 1993, Image Registration Between SAR and TM Data using DEM and Slant Range Information. *Proceedings of IGARSS -IEEE Trans. On Geoscience and Remote Sensing Symposium*, N**3**, 1351-1353.

Ton, J., and Jain, A.K., 1989, Registering Landsat images by point matching. *IEEE Trans. of Geoscience and Remote Sensing*, **27(5)**:642-651.

Ton, J., and Jain, A.K., 1989, Registering Landsat images by point matching.- *IEEE Trans. of Geoscience and Remote Sensing*, **27(5)**:642-651.

Toth, C.K., and Schenk, T., 1992, Feature based matching for automatic image registration, *ITC Journal* (**1**):40-46.

Vasileisky, A.S., and Berger, M., 1998, Automated Co-Registration of Multi-Sensor Images on the Basis of Linear Feature Recognition for Subsequent Data Fusion, *Proc. Conf. of Fusion of Earth Data*, Ecole des Mines de Paris, Sophia Antipolis, France, 59-65.

Vasileisky, A.S., and Maximov, N.A., 1993, Image processing technology for remote sencing.- *Proceedings of the 1993 MAI/BUAA international symposium on Automatic control.*, Moscow, Vol.**1**, Part 2, 38-42.

Ventura, A.D., Rampini, A., and Schettini, R., 1990, Image registration by the recognition of corresponding structures, *IEEE Trans. On Geoscience and Remote Sensing*, **28 (3)**:305-314.

Wong, R.Y., and Hall, E.L., 1978, Sequential hierarchical scene matching, *IEEE Trans.Comput.* Vol.**C-27**, 359-366.

Wu, Y., and Maitre, H., 1990, A multiresolution approach for registration of a SPOT image and a SAR image. *Proceedings of International Geoscience and Remote Sensing Symposium*, 635-638.

Zheng, Q., and Chellappa, R. A., 1993, Computational vision approach to image registration. *IEEE Trans. On Image Proc.*, **2(3)**:311-326.

Zhukov, B., Oertel, D., Berger, M., Kaufmann, H., and Müller, A., 1998, Unmixing and Fusion of Multi-Sensor Multi-Resolution Data acquired over the Makhtesh Ramon Negev Desert, *Proc. Conf. of Fusion of Earth Data*, Ecole des Mines de Paris, Sophia Antipolis, France, 135-140.

Anhang: Sachbericht IKI

A1: Image Registration using an Iterative Approach for Control Points Identification

A1.1 Iterative approach for control points identification

The proposed technique is based on the area-based method. It can be applied when images are preliminary transformed to projections with small differences in rotation angle and in scale. Tests have shown good results if the difference in scale is less than 10% and the mutual rotation angle is not higher than 8°. The technique automatically detects CP coordinates. Further, the manual involvement of an operator can be applied if desired. The operator has to confirm or to reject the automatically detected CPs.

A1.1.2 Preliminary transformation of images

Consider two registered images I(x,y) and J(i,j), where I(x,y) has the scale s_i, and J(i,j) - s_j. The image with the lower spatial resolution will be called reference image, the image with the higher spatial resolution will be called as the transformed image. Let $s_I > s_J$ then I(x,y) is the reference image and J(i,j) is the transformed image. The preliminary transformation is the following:

- the transformed image is turned to the projection, approximately parallel to the projection of the reference image;
- image J(i,j) is scaled to the resolution ~s_I, the result is $J_s(x,y)$;
- image I(x,y) is scaled to the resolution ~s_J, the result is $I_b(i,j)$;

The transformation is performed with the knowledge of the mutual disposition and the resolution of the imaging systems, if available. A rough estimation of the scale and the rotation angle can be defined by the feature-based method or manually. The bilinear or the cubic spline interpolation is used for the transformation.

A1.1.3 Window selection for matching

The reference image I(x,y) is split into fixed windows w(x,y) with a size of fnl*fns, as shown in fig.2.1. The entropy of intensity distribution is calculated of each window:

$$H = -1 / N \sum_{i=0}^{N} p_i * \log(p_i) \qquad (2.1)$$

where: N - the number of possible intensity values,
p_i - the number of pixels with intensity i.

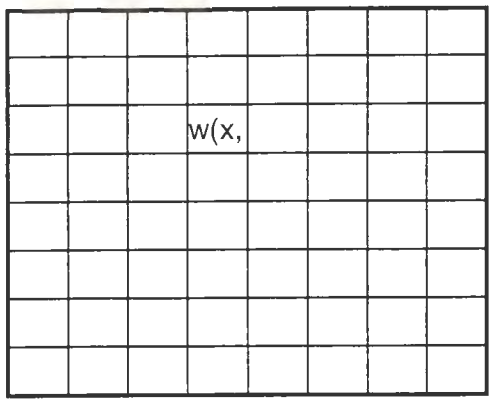

Fig.2.1. Windows on the reference image.

The entropy (2.1) is a function of the local histogram shape, it shows the homogeneity of the distribution. The windows with heterogeneous distributions (large value of H) are better to be used for the proposed method. All $w_i(x,y)$ are arranged in diminishing entropy order, so $w_0(x,y)$ has the maximum value of H, $w_1(x,y) < w_0(x,y)$, $w_2(x,y) < w_1(x,y)$, etc. One window is used for one pair of CP identification. The window of reference image is fixed and the search of a similar window on $J_s(x,y)$ is started.

A1.1.4 Steps of CP coordinates detection

The procedure of CP coordinates detection consists of three steps. Each following step increases the accuracy of the coordinate values, that is why the procedure is called the iterative approach. The small scale images I(x,y) and $J_s(x,y)$ are analyzed at the first step. The similar windows are detected with the accuracy of 1/2 of the window size. The correlation coefficient in the Fourier spectrum's domain or in the spatial domain, or the comparison of an integral power for circle frequency zones are used to detect corresponding windows of both images. The used algorithms are described in detail in 2.1.5.
Identical windows are determined by the second step with the accuracy less than one pixel of the low resolution image. The comparison algorithm works only over the region of $J_s(x,y)$, which is defined by the first step, but not over the whole transformed image. The CP coordinates for J(i,j) are defined by the third step with the accuracy of one pixel of the high resolution image. The comparison algorithm works only over the region of J(i,j), which is defined by the second step. The detected CP coordinates are stored and the process is repeated for the next window $w_n(x,y)$.

A1.1.5 Search of similar window over the transformed image

After the window $w_n(x,y)$ of the reference image is fixed, the scaled transformed image $J_s(x,y)$ is split into windows of the same size fnl*fns by the same way as the reference image

(Fig.2.1). Each window $v_m(x,y)$ is compared to $w_n(x,y)$ using a comparison algorithm. The resulted matching metrics R_m are arranged in diminishing order (e.g. R_0 is the largest value). The parameter R_m corresponds to each window $v_m(x,y)$ so that there is a set of $v_m(x,y)$ ranged in the order of their similarity to $w_n(x,y)$. The translation for $v_m(x,y)$ relative to $w_n(x,y)$ is not larger than fnl/2 in the line direction and not larger than fns/2 in the column direction. Thus the region V(x,y) used for searching corresponding windows $v_m(x',y')$ can be limited by $x \in (x'\text{-fnl}/2, x'\text{+fnl}/2)$, $y \in (y'\text{-fns}/2, y'\text{+fns}/2)$, as shown in Fig.2.2.

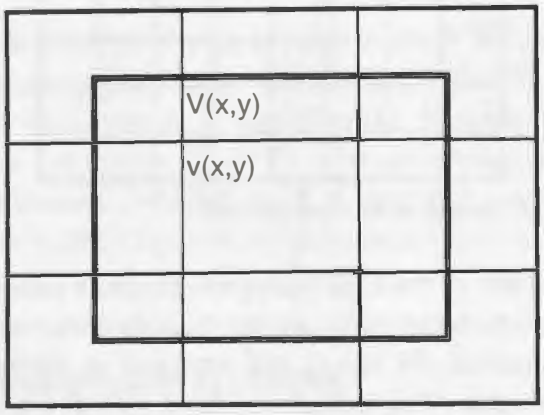

Fig. 2.2. The area V(x,y) for windows matching by the second iteration.

The window $w_0(x,y)$ of the image I(x,y) is compared to all possible windows $v_m'(x,y)$ of the image $J_s(x,y)$ over the region $V_0(x,y)$, defining $v_0(x,y)$ with corresponding R_0. The matching procedure is based on the correlation coefficient (CF) in the spatial domain for $w_n(x,y)$ and $v_m'(x,y)$. The window $v_0'(x,y)$ with its corresponding maximum CF R_0' is stored. Then the next window $v_1(x,y)$ is used to fix the search area $V_1(x,y)$. The window $v_1'(x,y)$ with its corresponding maximum CF R_1' is stored etc. The algorithm variable parameter N defines the number of areas to be matched at the second step. The window $v_m'(x,y)$ with the maximum R_m' provided after N attempts is considered to correspond to $w_n(x,y)$. An other rule to finish the calculations is if R_m' exceeds a given threshold R_{max}. The central point coordinates of the windows $w_n(x,y)$ and $v_m'(x,y)$ are used as CP coordinates for the low resolution matching. The next ranged window $w_1(x,y)$ is used to detect coordinates of the next CP as described above. The procedure is repeated for a number of desired CPs given by the operator.

The final step is performed using the high resolution images $I_b(i,j)$ and J(i,j). The detected by the previous steps coordinates x,y are transformed to i,j using a multiplication by the factor $s_{IJ} = s_I/s_J$. The window $w_n(i,j)$ is fixed in the reference image $I_b(i,j)$, which corresponds to already defined CP on the low resolution image I(x,y) and has a size fnl'*fns' (fnl'> s_{IJ}, fns'> s_{IJ}). The area $V_n(i,j)$ around the window $v_n(i,j)$ is defined in the transformed image J(i,j), the coordinates $v_n(i,j)$ corresponds to the CP coordinates for $v_m'(x,y)$. The size of $V_n(i,j)$ is defined as following: i should be in the range $(i\text{-}s_{IJ}, i\text{+}s_{IJ})$ and j should be in the range $(j\text{-}s_{IJ}, j\text{+}s_{IJ})$, so that the region is similar to that shown in Fig. 2.2. CF in spatial domain is calculated for the window $w_n(i,j)$ and every $v_m(i,j)$ over the area $V_n(i,j)$, and the window $v_m'(i,j)$ with the largest R_i is considered as the best match. The central point coordinates are fixed as CP coordinates for the transformed image J(i,j). The procedure is performed for the desired number of control points.

The CP coordinates for image I(x,y), fixed at the second step, and the CP coordinates for image J(i,j), fixed at the last step, are the final result. They are used to determine the mapping function.

A1.1.6 The algorithms of windows match at the first iteration

Three algorithms are proposed for a comparison of the windows for I(x,y) and $J_s(x,y)$. The first one is based on the analysis of correlation coefficient for Fourier spectra of the matching windows. The discrete Fourier transforms W(m,n) and V(m,n) are calculated for windows w(x,y) and v(x,y). Their correlation is given by:

$$R_f = \frac{\sum_m \sum_n |W(m,n)| * |V(m,n)|}{\sqrt{\sum_m \sum_n W^2(m,n)} * \sqrt{\sum_m \sum_n V^2(m,n)}} \qquad (2.2)$$

where: |W(m,n)|, |V(m,n)| - power Fourier spectra for w(x,y), v(x,y).

Fourier spectrum is invariant to a translation. Thus the translation of v(x,y) relative to w(x,y) caused by a fixed division of $J_s(x,y)$ has no influence to R_f. The best match of v(x,y) and w(x,y) corresponds to the maximum R_f.
The second algorithm is based on the property to preserve energy in the power Fourier spectrum in case of rotation and translation inside of circle zones. The following formula is used for analyzing windows:

$$E_w = \sum_m \sum_n W^2(m,n) \text{ and } E_v = \sum_m \sum_n V^2(m,n) ,$$

where: $m \in (m_s, m_e)$, $n \in (n_s, n_e)$ belong to the circle zone, as shown in fig.2.3. It is possible to use only a half of this zone, due to the fact that the Fourier power spectrum of pixel's real numbers is symmetric relative to origin. The Minimum of $R_s = |E_w - E_v|$ is taken as the best match for windows w(x,y), v(x,y).
The third algorithm determines the correlation coefficient of two windows in the spatial domain

$$R_f = \frac{\sum_m \sum_n |w(x,y)| * |v(x,y)|}{\sqrt{\sum_m \sum_n w^2(x,y)} * \sqrt{\sum_m \sum_n v^2(x,y)}} \qquad (2.3)$$

The best match of v(x,y) and w(x,y) corresponds to the maximum R_f.
M windows $v_m(x,y)$ of the transformed image $J_s(x,y)$ are stored for the second step.

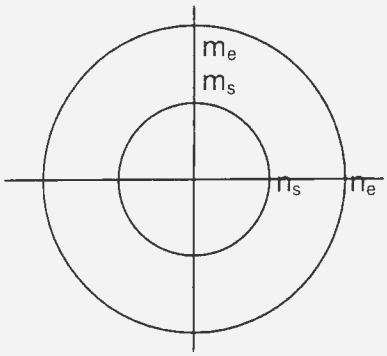

Fig. 2.3. Circle zone of Fourier power spectrum for energy calculation.

A1.1.6 Control point coordinates adjustment with subpixel accuracy

The CPs coordinates for I(x,y), $J_s(x,y)$ as defined at the second step of the iterative procedure are adjusted with subpixel accuracy if the intensities of registered images can be represented as:

$$\sum_s i = kI + b \quad (2.4)$$

where: *i* - intensity of the transformed image J(i,j), *I* - intensity of the reference image I(x,y), *s* - is the scale factor $s=s_J/s_I$, *k* - is a relative gain for the sensors, *b* - is a relative offset for the sensors providing the images.

The CP coordinates of J(i,j) are calculated by multiplying the defined CP coordinates of $J_s(x,y)$ by the scale factor $s_{IJ}=s_J/s_I$. The relative disposition of the surface area, which intensity contributes to pixels i of the transformed image and pixel I of the reference image can be presented as shown in Fig.2.4 (an example for one dimension).

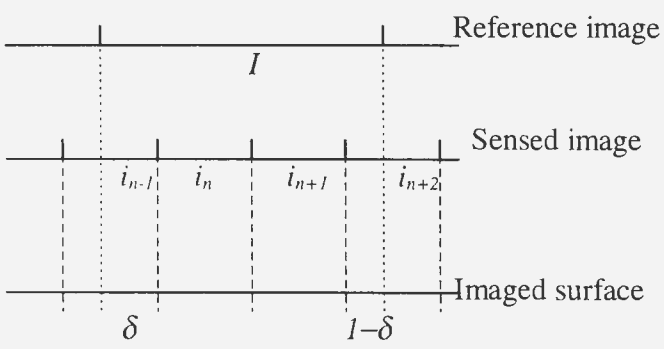

Fig.2.4. Mutual disposition of the pixels of registered images ($s_{IJ}=3$).

Each pixel represents the integral intensity of the imaged area, wich size depends on the sensor resolution. Therefore if δ is a translation value for J(x,y) relative to I(i,j), (2.4) is transformed to

$$\delta * i_{n-1} + \sum_{s-1} i_n + (1-\delta) * i_{n+1} = k * I + b$$

A similar equation can be constructed for two-dimensional case, using d_x for the translation in the line direction and d_y for the translation in the column direction. A system of these equation can be constructed for N control points and transformed to

$$a_{0i} + a_{1i} * \delta_x + a_{2i} * \delta_y + a_{3i} * \delta_x * \delta_y = k * I_i + b \qquad (2.5)$$

where: i=0,N-1 - CP number,

a_{ji} - coefficients, calculated for the environment of i-th CP area: $a_{0i} = \sum_{s-1} \sum_{s-1} i_{nm}$,

$a_{1i} = \sum_{s-1} i_{sm} - \sum_{s-1} i_{0m}$, $a_{2i} = \sum_{s-1} i_{ns} - \sum_{s-1} i_{n0}$, $a_{3i} = i_{00} + i_{ss} - i_{0s} - i_{s0}$

The solution of (2.5) relative to d_x, d_y, k, b gives an estimation of the mutual translation. The system of N equations (2.5) is overdeterminated for N>4 and least square method is used to define d_x, d_y, k, b. Thus the influence of brightness interpolation and of noise is decreased.

A1.1.7 Possible manual participation in the procedure

Interactive manual operations can be included in the proposed technique. The task of an operator is to select the algorithm to be used and to fix the number of desired CPs. The manual involvement makes it possible to speed up the procedure. The following possible interactive involvement can be considered.

1. Rejection of the reference image windows. An operator selects the reference image window w(x,y) for matching from the list, proposed by the algorithm. In this way the matching procedure, which takes much of computer power, can be eliminated for windows, which are located close to image boundaries and close to each other or which are placed on nonoverlapped areas of the registered images.
2. Rejection of wrong CP. The fixed w(x,y) and the produced at the second step v'(x,y) are displayed. An operator confirms or rejects the proposed by algorithm windows for the third step.
3. Speeding up control points identification. The window v'(x,y) is determined using the matching algorithm by the first step, w(x,y) and v'(x,y) are displayed. The operator confirms the result of the matching and starts the next step or can change the algorithm used to match the windows.

A1.2 Co-registration of the images

A1.2.1 Spatial transformation of the transformed image to the reference image.

The mapping function f(j,j) is calculated using the defined CP coordinates. A polynomial function is used to calculate the transformation of the registered images:

$$f(i,j) = a_0 + a_1 i + a_2 j + a_3 i^2 + a_4 ij + a_5 ij + a_6 j^2 + \ldots \qquad (2.6)$$

The polynomial degree t is defined by the number of CP - $n \geq (t+1)^2$.

The polynomial coefficients a_i are calculated using the least square method from the following system of equations:

$$x_k = \sum_l \sum_m a_i i_k^l j_k^m, \quad y_k = \sum_l \sum_m a_i i_k^l j_k^m \qquad (2.7)$$

with x_j, y_j, i_j, j_j are known CP coordinates. The transformation

$$J'(x,y) = J(f(i,j), f(i,j))$$

is performed to get the transformed transformed image. Bilinear or cubic spline interpolation is used for J'(x,y) pixel's value determination.

An other approach is based on triangulation. A set of CP coordinates for the reference image I(x,y) is considered as the coordinates of an irregular grid on the plane (x,y). The Deloney triangulation is determined over this grid [2.1,2.2]. The irregular grid on the plane (i,j) is constructed with using the result of triangulation and a set of CP coordinates for the transformed image J(i,j). This image is transformed over this grid with using linear or spline interpolation [2.1].

A1.2.2 Estimation of image co-registration accuracy

An estimation of co-registration accuracy is used to check the magnitude of residual co-ordinate difference between the transformed and the reference images. False CPs, errors in CP coordinates determination and invalid mapping functions are the source of the registration errors.

Consider the algorithm of accuracy estimation for the polynomial function (2.6). N CPs are required to calculate the coefficients a_i of this function. If images have local distortions then the co-registration errors can be caused by using a single mapping function for whole image. To decrease the errors the images I(x,y), J(i,j) are subdivided into polygons with N nodes and the coefficients of mapping functions are calculated for each polygon. The error estimation is performed using additional CPs, fixed on both images and not applied for polynomial construction.

The coordinates x', y' of an additional CP are defined using (2.7) with coefficients a_i, determined by the nodes of the polygon, with the extra CP inside. These additional point coordinates are compared with the CP coordinates on the reference image I(x,y). The absolute error for the polygon window is the difference:

$$\Delta_x = x' - x_r \; ; \; \Delta_y = y' - y_r$$

where: x_r, y_r - the actual coordinates of additional CP in the reference image.

The mean square root errors are calculated on the base of the absolute errors:

$$m_x = \sqrt{\frac{\sum \Delta_x^2}{n-1}} \; ; \qquad m_y = \sqrt{\frac{\sum \Delta_y^2}{n-1}}$$

where: n – the number of the additional CPs.

Another method of registration errors estimation is the following. The transformed image J(x,y) is transformed by the mapping function, whose coefficients are obtained using the nodes of a polygon in a similar way as described above but in this case each polygon has N+1 nodes.
The N+1 systems of equations (2.7) are obtained for each CP set. The unknown coefficients a_i are calculated as the solution of the system of 2*(N+1) equations using the least square method. The error estimation is possible due to the extra CP, which gives 2 additional equations (2.7). The mean square root error μ estimates the registration accuracy:

$$\mu = \sqrt{\frac{\sum_{i=1}^{2(N+1)} V_i^2}{2}} \; ,$$

$$\text{where: } V_i = \begin{cases} \sum_i a_i \cdot i \cdot j - x' & \text{for odd } i \\ \sum_i b_i \cdot i \cdot j - y' & \text{for even } i \end{cases}$$

The procedure is performed for all polygons.
The advantage of this approach is the possibility to get the information about each CP (false or true) using different values of V_i, and to reject the false CP. The last procedure increases the registration accuracy, because only the true CP are used for co-registration.

A1.2.3 Application to multispectral images

The iterative technique can be applied properly to images I(x,y), J(i,j) if their histograms are related as:

$$p_I(k) = ap_J(k) + b,$$

therefore it's desirable that both registered images have at least one channel with a similar spectral band. Many sensors use the same front optics or have the parallel axis optics for different channels. All channels for such cameras provide an identical projection of produced images. The iterative approach can be applied using the similar bands. CPs are identified using these bands and then the other band images are registered by the defined CP coordinates.

A1.2.4 Specification of the program for image co-registration

SW program was developed based on the presented iterative technique. The program was written on IDL for UNIX workstation and widgets [2.3] are used for graphic user interface. The program provides the operations with two single-band images of GIF format or binary pure images (ENVI format). The program performs the following operations: CP determination on the base of the iterative method, described in topic 2.1, the transformation of the transformed image to the reference image projection using the existing IDL mapping functions with coefficients, calculated using the determined CP; display of transformed and reference images with determined CPs. The program provides additional operations for preliminary image transformations - image fragment extraction, image rotation, scale modification, image translation and image filtration using band-pass filter. These additional operations are based on the existing IDL functions and combined in one widget controlled program. The array of CP coordinates, transformed image or its fragment are the main results of the program application. The image processed by the preliminary transformation algorithm is the additional result.
Description of the widgets to control the program is presented below.
The main widget is the following:

file	processing	transformation	view	
Image Size				
define nl	512	define nc		512
Window size				
define wnl	32	define wnc		32
CP coordinates				
n:		y_{ref}	x_{ref} y_{sens}	x_{sens}

Image Size defines the size of the reference, the transformed or output image, depends on the user request to open the image in the *file* field: *nl* - number of lines, *nc* - number of columns. *Window Size* defines the window size for CP identification. *CP coordinates* shows

the id number and coordinates of a control point. An editing is available in this field to provide the elimination of the false CPs. The corrected array of CP coordinates is stored after editing.

Widget *file* should be used for the following functions:

open reference image	make the reference image available for processing
open sensed image	make the transformed image available for processing
open output image	define the output image for result of transformation
open CP array	make CP array available for image transformation
save output image	store the produced image in a file
save CP array	store the produced CP array in a file
close sensed image	end the opportunity to use the transformed image
close reg. image	end the opportunity to use the reference image
close output image	end the opportunity to use the output image
quit	close all widgets and exits from the program

The *nl* and *nc* are specified for all three possible images, then the binary pure format is used. These parameters should be fixed for the output image of GIF format. The standard IDL widget is used to search and to specify filenames. It should close the image or save CP array before starting work with a new source file.

Widget *processing* looks as:

parameters	define the iterative algorithm parameters
CP search	define CP coordinates on low resolution images
adjustment	Define CP coordinates on high resolution images with a pixel accuracy
subpixel adj.	Define CP coordinates on high resolution images with a subpixel accuracy

The *parameters* create a modal widget for algorithm parameters specification. *CP search* performs the first and second iterations of the algorithm and identifies the CPs coordinates for low resolution images. *Adjustment* and *subpixel adj.* performs the third iteration and defines the final CP coordinates for transformed images.

The modal widget for parameters specification looks like the following:

Start Algorithm				
	FFT COR	INT COR	SP DIFF	
define N of CPs:		15		Reset CP
define N of steps		5		
define threshold		0.75		
define start window		0		
Frequency Zone Size				
define sb	4	define fb		24

Relative Scale			
define scl	2.5	define scc	3.2
DONE			

Start Algorithm determines what algorithm will be used ae the first at the first iteration: *FFT COR* - correlation coefficient analysis of Fourier spectrums, *INT COR* - correlation coefficient analysis of windows in the spatial domain, *SP DIFF* - analysis of circular zones of power Fourier spectra. The next fields define the requested number of CP, the number of window N for matching by the second iteration, the threshold value R' to break the second iteration, the window id in the range to start the matching procedure. The button *Reset CP* resets the determined CPs sets the CP id to 0, and provides the new procedure of CPs identification for the current images. *Frequency zone size* defines a bandpass filter for a power spectrum circular zone: *sb* - start frequency, *fb* - final frequency. The frequencies can vary in the range of (0,n), n is the number of pixels in the image line. Relative scale defines the relative scale factor s by the line and by the column of image. The button DONE provides the exit from the module widget after the specification of the parameters.

Widget "transformation" has the following functions:

window	extract a window of the reference image
scale	modify the scale of the reference image
shift	shift the reference image
edges	extract the edges on the reference image
filtration	use a bandpass filter for reference image
mapping	transform the transformed image to reference image projection
rotation	rotate the reference image by the specified angle

The result of image transformations is stored in the output image, which should be opened before the operation. The window size is defined by the size of the output image. The left lowest point coordinates of the window is defined by the additional modal widget. The scale value is defined by the output image size. The translation is defined by the additional modal widget. Filtration frequencies are defined by *sb,fb*. The rotation angle is defined by the additional modal widget.

Widget "view" looks as:

load C T	change color table for display
refe r. image	display the reference image
se nse d image	display the sensed image
output image	display the output image
CP array	display and edit the array of control points

A1.2.5 Test application and results

The presented technique was tested to co-registrate the images, obtained by HRV SPOT, Landsat TM and JERS FUYO over the area of 'Ramon' desert. This area is characterized by large intensity variations due to surface crevices. The images produced by the panchromatic and by multispectral channels of the cameras with different spatial resolution were used for co-registration tests. The window size fnl,fns, the threshold value of correlation coefficient R' and the number of matching windows at the second iteration N were the variable parameters of the algorithm. The results are presented in Table 2.1. The accuracy was calculated after false CPs elimination. CP identification for images HRV pan and FUYO vis is shown at Fig. 2.5 and the co-registration of images HRV pan and TM vis is shown at Fig. 2.6.
The tests had shown a good performance of the iterative technique and the developed SW. The optimal parameter values are the following: fnl=fns=20-32, N=3-7, R'=0,65-0,75 (they depend on the radiometric resolution and overlapping of the registered images). The effective size of the circular zone for Fourier power spectra analysis is 0.13-0.6. The number of false CP is not higher than 10% for images with high and middle overlapping and not higher than 20% for images with low overlapping, including some CP on the boundaries of images. False CPs were eliminated by the operator working in the manual involvement mode.

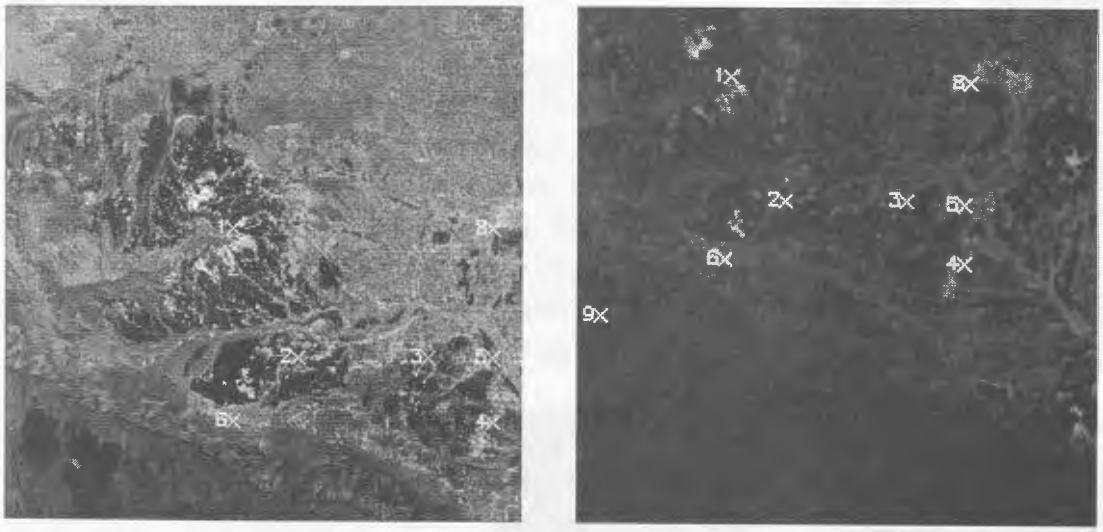

a) b)

Fig. 2.5 Control points identification for images b) TM vis and b) FUYO vis.

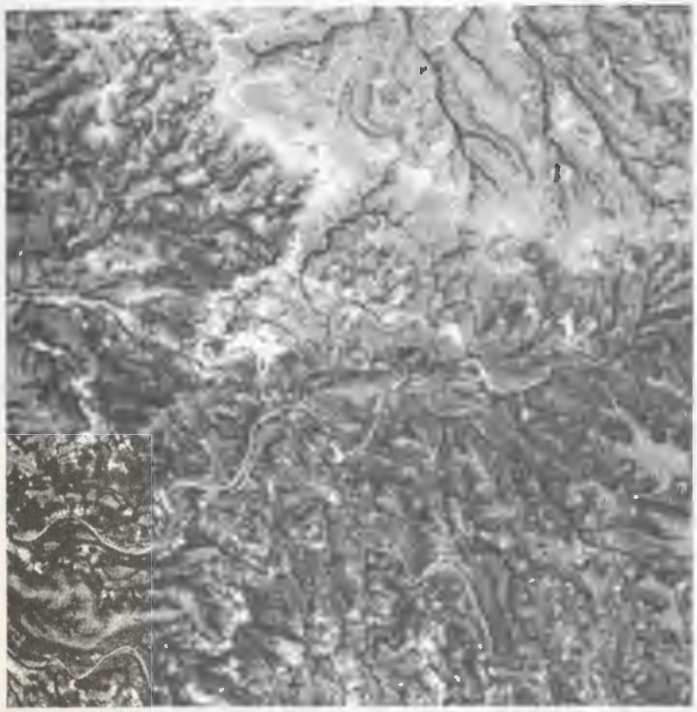

a)

b)

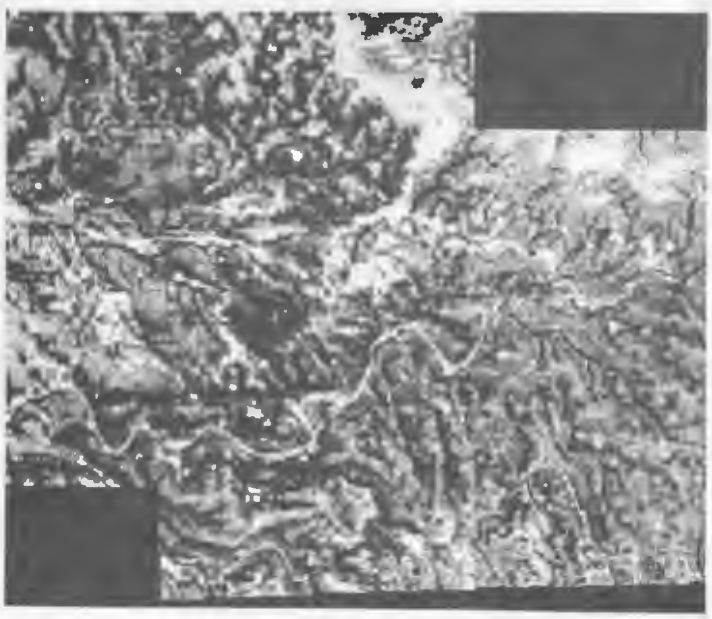

c)

Fig. 2.6. *The result image - c) of co-registration of HRV pan - a) and TM vis - b).*

Table 2.1

Images for co-registration, overlapping	Spatial and radiometric resolution	fnl,fns, N, R'	N of requested and false detected CP	Accuracy estimation	Computer time
HRV pan TM vis, middle	10x10m, 0.5-0.73 30x30m 0.45-0.52	32x32, 0.6 20x20, 0.55 16x16, 0.65	21/0 21/1 40/2	0.12 0.67 0.49	10 min. 6 min. 4.5 min
HRV xs vis TM vis, high	20x20m 0.5-0.59 30x30m 0.45-0.52	32*32, 0.75 16x16, 0.8	25/1 40/4	0.21 0.18	5.5 min. 8 min.
HRV pan FUYO vis, low	10x10m, 0.5-0.73 18*24 0.52-0.60	32x32, 0.7 16x16, 0.7	17/3 30/8	0.72 0.57	10 min. 12 min.
TM vis FUYO vis, low	30x30m 0.45-0.52 18*24 0.52-0.60	32x32, 0.8 20x20, 0.75 48x48, 0.7	17/2 17/4 15/3	0.73 0.92 -	30 min. 10 min. 40 min.
HRV xs vis TM blue, high	20x20m 0.5-0.59 30x30m 2.08-2.35	32x32, 0.75 16x16, 0.7	25/0 15/4	0.68 -	10 min. 11.5 min.
TM blue FUYO vis, low	30x30m 2.08-2.35 18*24 0.52-0.60	32x32, 0.75 22x22, 0.78	15/1 15/2	0.78 0.90	25 min. 15 min.

A1.3 Conclusions

The proposed iterative technique is applicable if the registered images can be transformed to the images slightly turned relative to each other, where the mutual turn angle is less than 8^0 grad. They should be reduced to approximately the same scale: the difference in the scale should be less than 10%. The iterative approach provides a flexible image registration procedure to achieve a higher accuracy. The optional manual involvement can speed up the procedure and makes it more accurate. The object oriented program module, which realizes the iterative technique, can be easily modified and updated by new algorithms.
It is planned to enhance the proposed technique in future as follows:

- development of the windows matching algorithms for images with any mutual rotation;
- development of a method of automatic detection of mutual rotation and of the difference in scale;
- analysis of application of the different window matching algorithms at the second and the third steps of the iterative technique;
- development and analysis of different mapping function used for the transformed image transformation to the reference image projection.

A large amount of experimental studies on image co-registration for different sensors have to be performed for estimation of co-registration accuracy and its sensitivity to various distortions of original images.

A2: Image Co-registration using Intersections of Linear Features

Borders of different areas and objects on the Earth surface form the base structure of this surface, well recognized on aerospace images. Most parts of these borders with limited length are straight lines or may be approximated by such lines. An important for image co-registration property of borders is the fact, that they are preserved on images in various spectral bands. Rectilinear features may be easily identified, and their orientation may be estimated with a high degree of accuracy. It makes it possible to develop accurate techniques for image co-registration, even in different spectral bands, on the base of linear control elements matching.
It is supposed in this work, that a preliminary rough images co-registration was performed using usually available apriori information (information on s/c orbit, time of imaging, camera characteristics, optical axis direction). The described technique is aimed at a high accuracy image co-registration with the use of only images itself, without any additional information on their spatial and radiometric parameters.

A2.1 Technique of image co-registration using intersections of linear features

A2.1.1 Brief description of co-registration technique

The proposed co-registration technique is based on selection and matching of image features such as intersections of rectilinear elements. The technique includes the following main steps: borders detection, control features selection, control features matching, estimation of the control points coordinates and final co-registration.

Borders detection

A preliminary step of the proposed image co-registration technique is the following. Borders detection is performed separately on both original grayscale images. The convolution of the images with the Laplassian mask may be used to detect sufficient brightness changes. After it, the obtained gradient images are thresholded to extract the pixels where brightness changes are greater than some given threshold. As a result of the preliminary step, images are converted into a binary form.

Control features selection

Control features are selected independently on both images at this step. Fragments with crossing rectilinear elements are used as control features. Such fragments are called control fragments. Hough transformation is used for rectilinear elements detection.
First of all, images are splitted for equal rectangular fragments of a given size. Hough transformation is performed for each fragment, making it possible to detect rectilinear

elements presence. Uniformity vector of brightness distribution in a Hough transform column is calculated for each fragment. It shows the power and inclination angle of straight lines present in a fragment (line power is the number of pixels forming this line). After it, a measure of crossing lines presence in each fragment is calculated. It makes it possible to find fragments with well expressed crossing lines. Some given number of fragments with the highest value of the measure are selected. These fragments are considered as control fragments. Automatic selection of control fragments makes it possible to use a lot of fragments, increasing co-registration accuracy.

Control features matching

At this step, the selected control fragments of the reference and matched images are compared, correspondence is established, and pairs of coincident control fragments are formed. Matching of coincident control fragments pairs is performed by comparison of fragments of the reference and matched images and by analysis of information on their relative location. Fragments are described by uniformity vectors for comparison. Relative location of fragments in an image is described by distances between fragment centers. Unsuccessfully matched fragments are discarded.

Evaluation of control points coordinates

Though the same place on the ground surface is imaged at matched fragments, these fragments may be rotated and shifted one relative to another. So, at this step, the angle of rotation and the value of horizontal and vertical translation of the fragments in selected pairs are evaluated. The centers of control fragments are selected at the reference image as control points for subsequent estimation of the transformation matrix. Control points are shifted from the center of the corresponding control fragments on the matched image by the evaluated shift value.

Image co-registration

Technique of the further transformation matrix evaluation according to control points coordinates and on algorithm of the matched image registration with the reference image are described in section 2.

A2.1.2 Hough transform usage for linear objects recognition

Statistical methods or convolution of the original image with a set of detection masks for corresponding directions may be used for extraction of linear border segments. However, extended border segments detection by such techniques require operations with masks of a large size, increasing severely the processing time. Moreover, statistical

techniques are quite complex; convolution with masks may not lead to good results in a case of weared and fractionated borders. Estimation of linear border segments direction with sufficient accuracy requires convolution with a very large number of masks, corresponding to detecting directions.

However, there is a technique capable to detect extended linear elements with a sufficient accuracy of estimation of their orientation and location. It does not require the border continuity and is not highly effected by various noise. Let us consider a technique of border points connection by determination of their deposition at lines of various direction. Assume, that there are N points on the plane (x,y). It is necessary to find subsequences of points belonging to straight lines. Let us draw the lines passing through each pair of points. After it, we find all closed lines and join points belonging to it into subsequences. This technique is very laborious, especially in the case of a large point number on the image. $N\ (N-1)/2$ lines have to be drawn and N^3 comparisons of points and lines have to be done according to it.

Another approach to a solution of this problem was proposed by Hough [3.1]. It is based on so called Hough transform. Let us consider a point (x,y) and the generalized equation of a line: $y = ax + b$. There is an infinite number of lines, passing through the point (x,y), but all of them satisfy the equation $y = ax + b$ with different *a* and *b* values. However, if one rewrites this equation as $b = -xa + y$ and look at the [A,B] plane called the parametric space, one will get the equation of one line for a given point (x,y). Moreover, a second point with (x_1, y_1) coordinates has its own line in the parametric space, and these two lines cross at a (a_1, b_1) point, where a_1 and b_1 represent parameters of the straight line that passes through two points (x,y) and (x_1, y_1). Correspondence of lines and points in the [A,B] and [X,Y] spaces is represented in Fig.3-1. If some points in the image space [X,Y] lies on one line, the corresponding lines in the parametric space [A,B] cross at one point, representing the coordinates of this line.

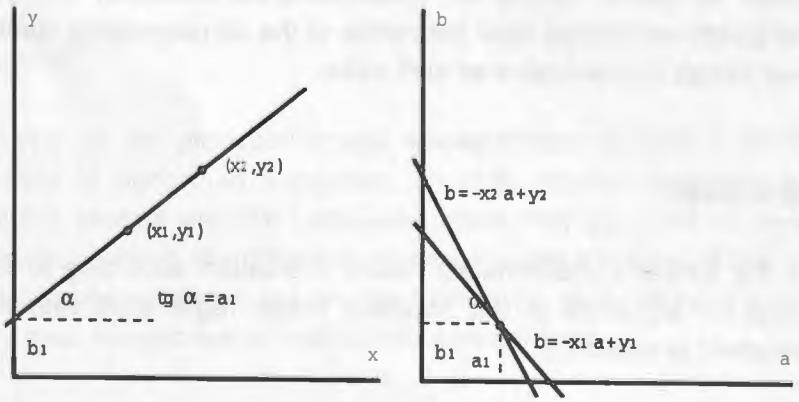

Fig.3-1. Correspondence of lines and points in the image space [X,Y] and the parametric space [A,B].

Initially Hough [3.1] proposed an analogue device for implementation of the described transform during recognition of linear particle tracks in a bubble chamber. A digital algorithm for transformation of an image from the image space into the parametric space is based on application of gathering units concept. The parametric space is splitting into gathering units. First, these units obtain zero values. Then, for each image point (x,y), we use all possible *a* values and get the corresponding *b* values using the

equation $b = -xa + y$. After it, the gathering unit corresponding to the pair (a,b) increments by one. Finally, after the procedure completion, the gathering unit value *M* represents *M* points on the corresponding line in the image space.
A volume of calculations for the digital Hough transform is *NK*, where *N* - the number of points in the image, *K* - the number of partitions at the A axis of the parametric space. This technique leads to a significant decrease of calculation time when the number of points is large. However, the described technique has significant disadvantage, that the parameters are infinite in the case when vertical straight lines are present in the image (because the tangent of 90° angle is infinite).
This difficulty can be removed by the usage of another parametric space, linked with the representation of a line in the polar coordinate system in the form:

$$x\cos\varphi + y\sin\varphi = \rho$$

The parameters ρ and φ are illustrated by Fig.3-2. ρ - distance from the origin to the line, φ - inclination angle of the line relative to the OY axis. Instead of the stright lines, we have sine curves in the parametric space. M points belonging to the line $x\cos\varphi_i + y\sin\varphi_i = \rho_i$ still correspond to *M* sine curves in the parametric space, crossing at the point (φ_i, ρ_i).

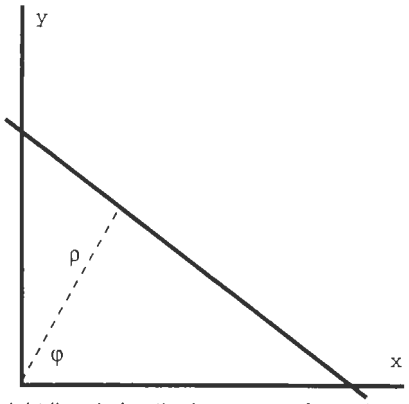

Fig.3-2. *ρ è φ parameters of a straight line during the image transformation into the parametric space of the polar coordinates.*

An algorithm, based on the described technique, is analogous to the discussed above. The parametric space is partitioned into gathering units, corresponding to a few degrees of line inclination angle and one pixel of distance to the origin. Note, that the part of the transformed image for the inclination angles 180-360° is fully analogous to that for the angles of 0-180°. It makes it possible to decrease the size of the parametric space and essentially save computer memory. Furthermore, not all gathering units inside a rectangular region of the parametric space have corresponding lines that pass through the given image. Many of them correspond to lines outside the viewing field. A rectangular region in the image space has a complex non-rectangular shape in the parametric space. However, an account of only the valid gathering units would lead to a complex coordinate recalculation and would increase inadmissible the calculation time. First of all during the transform, all gathering units get the zero values first of all. Then we scan the original image looking for all marked points. For each of such points, we build a sine curve in the parametric space according to the equation

$\rho = x\cos\varphi + y\sin\varphi$. Each gathering unit on this sine curve increments by one. It is not necessary to calculate sine and cosine values for each angle every time we perform the transform. Before the beginning of the calculation, the table may be built, consisting of sine and cosine values for each column of gathering units.

As a result, we get a rectangular image of Hough transform of the original scene. Each point of the original image corresponds to a sine curve with the brightness of one, while more bright places with intersection of many curves correspond to a straight line in the original image. Vertical lines correspond to bright concentrations near to the left or right border of the transformed image. Horizontal lines correspond to concentrations near the middle of transformed image.

Some examples of Hough transform are presented in Fig.3-3 and Fig.3-4. Fig.3-3 shows the Hough transform of a test image with five points. Each point corresponds to its own sine curve with brightness of one in the parametric space. Intersections of the curves correspond to some points belonging to one line. Bright concentration at the right part of the transform corresponds to a line, which passes through four points of the original image at once (points 1,3,4,5).

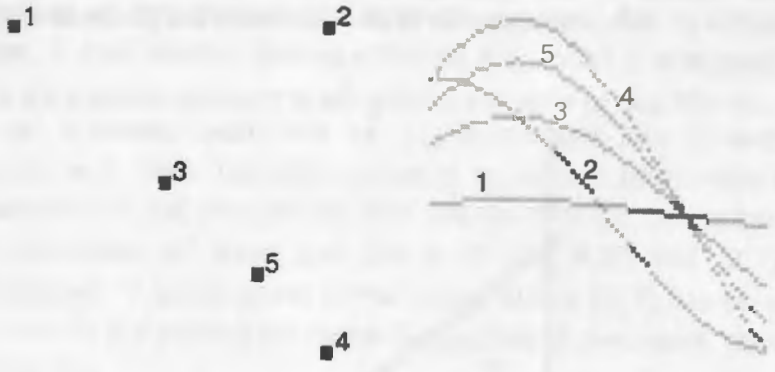

Fig.3-3. Test image with five points and its Hough transform.

Fig.3-4. presents a more complex image of Hough transform from some lines. The bright concentrations correspond to lines at the original image. Parallel lines transform into concentrations located one over another (for example, lines 5 and 6). Note that the right border of the transformed image may be joined with the left; it is necessary only to flip vertically one of them.

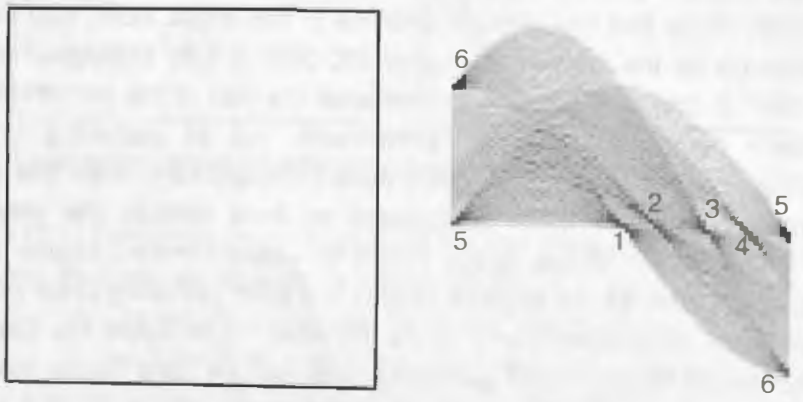

Fig.3-4. Test image with some lines and its Hough transform.

The main property of the Hough transform is that straight lines transforms into concentrations of bright points. Brightness of the gathering unit shows the number of points belonging to the corresponding line. Line coordinates may be obtained by search of local peaks in the parametric space in the region of concentration. Concentration brightness represents the power of a line. Assuming that significant for further consideration lines must be extended, we may perform thresholding of the transformed image and so reject all small line segments and noise points.
An advantage of Hough transform is its insensitivity to noise. Separate noise points practically do not affect the resulting transformed image. Stright image elements may have many breaks. Howewer, Hough transform does not give information on connection of linear segments and on positions of different segments. *F.O'Gorman* and *M.B.Clowes* proposed a modification of Hough transform without this disadvantage [3.2]. It is efficient to transform binary images with as few marked points as possible. It leads to an increase of the algorithm speed and to depression of noise components in the resulting image. To meet this requirement, it is necessary to increase the threshold during extraction of border elements. It is the difference of Hough transform based technique from other linear elements recognition techniques with the main requirement of line continuity.
Hough transform originally designed for recognition of straight lines may be generalized for detection of elements with nonlinear shape. Extension of this technique for the case of nonlinear elements was proposed by *Duda* and *Hart* [3.3]. However, due to a high complexity, we will not discuss this question.

A2.1.3 Estimation of the fragment rotation angle

The unique property of the Hough transform is the fact, that during rotation of original image on arbitrary angle around the origin its transform displaces along the X-axis by a shift, representing the angle of rotation. Indeed, if a line rotates around the origin, only the angle of inclination varies, but the distance to the line remains constant. Therefore, if we have two images rotated one relative to another around the origin, then in order to estimate the angle of rotation, it is only necessary to co-register two images of Hough transform by a simple shift along the X-axis. Co-registration may by performed by one of correlation techniques, but volume of calculations will not be large, because the shift have to be performed only along one axis. Taking into account quite low sensitivity of Hough transform to noise, we can estimate similarity of two images that differ a little and also to estimate the angle of rotation between them.
Regretfully, the technique is much more complex in a case of image rotation around any other point, but the origin. In this case Hough transform of an image not only displaces along the X-axis, but a complex shift up or down of each column of the transformed image takes place according to the sine curve. Indeed, Fig.3-5 shows that during rotation of a line around any arbitrary point, the distance from the origin to this line varies as a function of the line inclination angle.

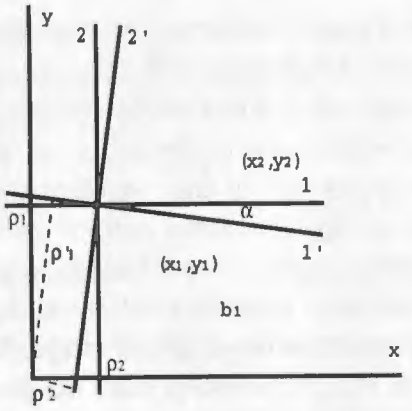

Fig.3-5. Effect of image rotation around an arbitrary point on Hough transform of this image.

Fig.3-6 shows two test images, rotated one relative to another and their Hough transform. Hough transform shifts along the X-axis cyclically: the columns shifted out from right border appear in the left. Each transformation column also shifts vertically according to the complex sine curve.

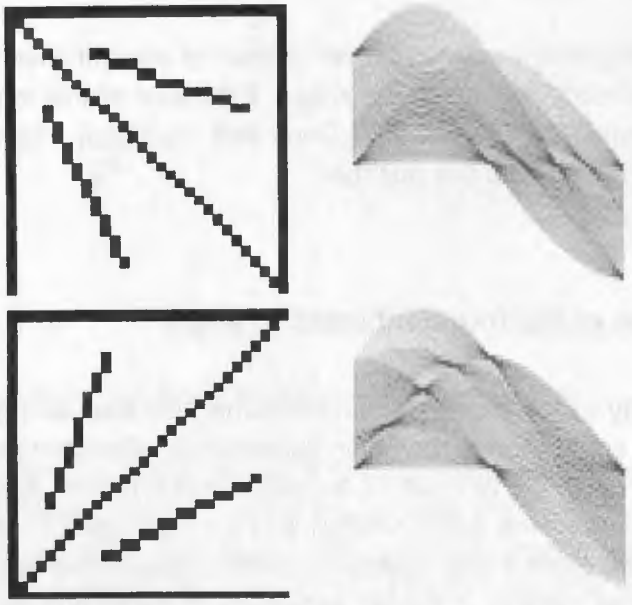

Fig.3-6. Two test images, rotated one relative to another by 90° angle and their Hough transform.

However, note that the transformed image itself still shifts along the X-axis by a value, corresponding to the angle of original image rotation, and the columns of the transform shift vertically. Thus, if one would characterize each column of the transformed image by some variable independent the from vertical shift and characterizing only the structure of brightness distribution in column, then the image would be represented by a rotation-invariant vector. The size of this vector will be equal to the size of the transformed image (the number of distinguishable directions on the original image). Rotation of original image around any point would lead to a shift of this vector right or left, taking into account that the vector is cycled and its right border is joined with the left.

A sum of elements of each column of a Hough transformed image is constant and equal to the number of points in the original image *N*, so the sum of squared column elements

seems to be a good characteristic of brightness distribution in columns. This variable gets the maximum value of N^2, if all brightness in a column is concentrated in one point. In the case of a uniform brightness distribution along the column, this value is equal to N. Let us call this variable as uniformity of brightness distribution in a column of Hough transform. Usage of the normalized uniformity vector for image co-registration was proposed by *A.S.Vasileisky* and *N.A.Maximov* [3.4]. Normalized uniformity of brightness distribution for i-th column is calculated according to the following equation:

$$O_i = O(\varphi_i) = \frac{1}{N} \sum_{j=0}^{k} A^2(i, j)$$

and varies from 1 to 1/N, where k - size of column, $A(i, j)$ - brightness of element j of i-th column in Hough transform.

Fig.3-7 presents charts of normalized uniformity vectors calculated from Hough transforms of the images shown in Fig.3-6. The left of the original images is also shown in Fig.3-4. The peaks on these charts correspond to columns of Hough transform, that illustrate concentrations of brightness and consequently of lines in the original image. The peak coordinates represent the inclination angle of lines in the original image.

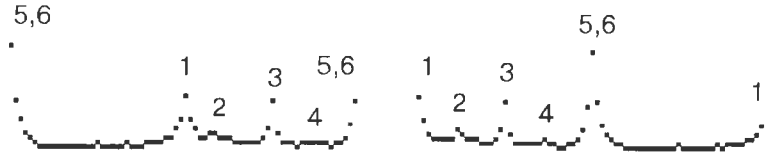

Fig.3-7. *Charts of normalized uniformity vector of brightness distribution in Hough transform columns; the original images are shown in Fig.3-4 and Fig.3-6.*

So, for estimation of the rotation angle of one image relative to another similar image, it is necessary first to perform Hough transform for both images. Then for each transformed image we must calculate the uniformity vector and determine the shift value of one vector relative to another that gives the minimal differences between its elements. The difference may be estimated by the correlation coefficient, calculated according to the equation:

$$K(l) = \sum_i O_1(i) O_2(i + l)$$

where $O_1(i)$ and $O_2(i)$ - uniformity vector elements. After it, the value of the best shift l gives the estimation of the rotation angle of one image relative to another.

A2.1.4 Estimation of fragments translation value

Another value to be estimated during co-registration of two images is a translation of an image relative to another. Rotation of image around an arbitrary point may be compensed by back rotation by the same angle around the origin and by a consequent translation by some shift. It is necessary to estimate the shift of each column of Hough transform of the original and transformed image to get this value of translation. It was already noted that the of vertical column shift depends on its position on X-axis according to some sine function. Each sine curve in the parametric space during Hough transform has a corresponding unique point in the image space. We can get the two required shift values by estimation of the sine function parameters, namely, by application of the back Hough transform.
A technique of shift value estimation is the following. First, after the Hough transform and taking into account the horizontal shift, corresponding to the rotation angle of one image relative to another, we estimate vertical shift of image columns. Estimation of these shifts may be carried out using a correlation technique. We find a relative shift that gives the maximal correlation of two columns. Then the collected vector of sine function of the shift values is processed according to the least squares technique. As a result, we find parameters of sine function:

$$\Delta\rho_i = x\cos\varphi_i + y\sin\varphi_i$$

These parameters *(x,y)* represent an estimation of one original image translation relative to another.

A2.1.5 Automated selection of control fragments with intersections of linear features

Structure techniques of image co-registration are based on recognition and matching structure elements in images - so called control features. The proposed technique is based on using intersections of linear elements in images as control features. A control fragment - an image fragment with a control feature - must contain at least two extended linear features, crossing at an angle close to 90°.
Intersections of roads, rivers, field borders and other linear extended objects may be examples of control features. Let us state requirements for a control fragment:

- The fragment must contain at least two linear extended objects. In a case of presence of one distinguishable linear object we can perform image co-registration only in the direction normal to this object.
- These objects must be sufficient long. Orientation of extended objects may be estimated with a high accuracy.

- Linear objects must crosses at an angle close to 90°. Presence of two parallel objects without crossing point makes co-registration possible only in the direction, normal to these objects. Angles from 30° to 90° are preferable for co-registration.

It is necessary to use a large number of control fragments during image co-registration to increase accuracy, especially in the case of geometric non-linear distortions. These fragments must be distributed uniformly over the image. A manual control features selection by an operator for co-registration is quite laborious and prolix. So, it is preferable to develop an automated technique of control features selection.
To make the process of control feature selection automated, it is necessary to develop a fragment measure, that would make it possible to select fragments, best meeting the listed requirements. This measure must get a high value in the case of two crossing features presence in a fragment.
The described uniformity vector of brightness distribution in a Hough transform column may be used for development of such measure. A peak in a uniformity vector reports about a presence of an extended line in the image in the corresponding direction. Uniformity vector analysis makes it possible to detect line in a fragment and to estimate their directions.
The following measure for a fragment is proposed:

$$E = \max_{\varphi=0,\psi=0}^{\pi} \left[O(\varphi) \cdot O(\psi) \cdot K(\varphi - \psi) \right] ,$$

where $O(\varphi)$, $O(\psi)$ are values of uniformity vector for directions φ and ψ correspondingly; $K(\varphi - \psi)$ - weight coefficient. The value of the weight coefficient must be equal to zero if φ and ψ are the same and 1 in the case when the angle between φ and ψ directions is equal to $\frac{\pi}{2}$. The weight coefficient may be of the following form, satisfying the stated requirements:

$$K(\varphi - \psi) = \frac{1}{2}\left[\sin\left(2 \cdot abs(\varphi - \psi) - \frac{\pi}{2} \right) + 1 \right]$$

Fig.3-8. Form of the weight coefficient $K(\varphi - \psi)$.

Dependence of the weight coefficient from the angle between directions φ and ψ is presented on Fig.3-8. The described measure makes possible the detection of two peaks in uniformity vector and so recognition of two extended straight lines in a fragment. Weight coefficient usage provides a selection of only sufficiently non-parallel lines. Thus, the higher the measure value is, the more probable is presence of two crossing lines in the examined fragment.

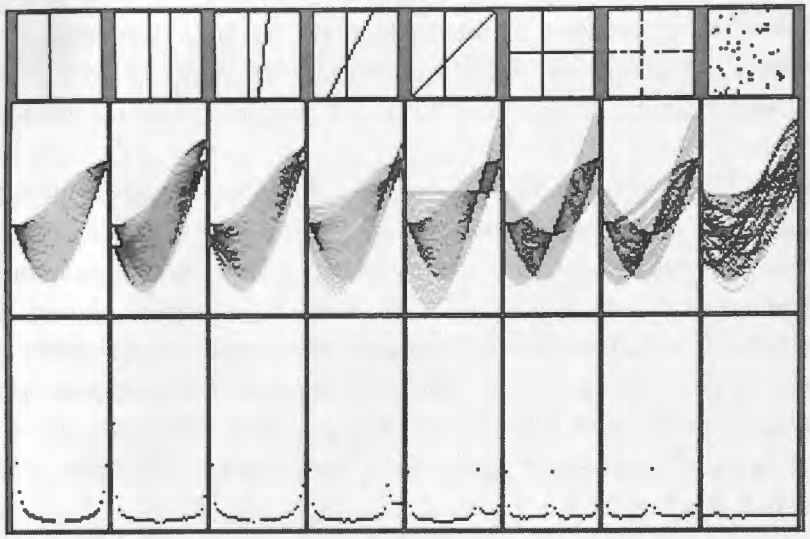

Fig.3-9. Test images, corresponding uniformity vector charts and calculated measures of crossing lines presence.

Fig.3-9. presents some examples of calculation of the proposed measure for some test images. This figure shows original images, uniformity vectors and $K\ (\varphi - \psi)$ charts for the fixed value φ=0, corresponding to the vertical line, drawn on all images. The presented example indicates that the measure of crossing lines presence in a fragment gets considerable values in the case of the angle between crossing lines from 30° to 90°. Regretfully, the proposed measure depends in the number of points on the original image. Image fragments containing only a few points usually give a high measure. Really, if only three points present at the image, then such image may be considered as three lines of two points each. All points belong to these lines, so the measure of crossing lines presence is quite high. But such fragment is not useful for consequent co-registration. Hence, it is useful to bolt out fragments with few points during fragment selection for consequent co-registration besides taking into account this measure of crossing lines presence.

A2.1.6 Control fragments matching

The technique to detect crossing lines in fragments described above makes possible a process of automated selection of control fragments with distinctive crossing linear features from images. So, we can select a set of useful fragments from each of the images to be co-registrated. As already noted, it is preferable to select a high number of control fragments for co-registration with high accuracy, and these fragments have to be distributed uniformly over the image. The next step of co-registration process is fragments matching. Uniformity vectors of fragments may be used for matching in our case besides the information on fragments co-location. Indeed, the normalized uniformity vector describes lines presence in a fragment in different directions. It is quite compact and informative at the same time. We can compare the selected fragments and find similar by comparing uniformity vectors. Comparison process is performed according to a correlation technique.

Let us consider two images A and B. First we select image fragments with a high measure of crossing lines presence. The number of selected fragments n_1 and n_2 may be different in these two images. Uniformity vectors $O_{A,i_1}(k)$ and $O_{B,i_2}(m)$ are calculated for the selected fragments, where A and B correspond to fragments belonging to one of the images; i_1 and i_2 - fragment numbers. Let us calculate the correlation matrix $K_{AB}(i_1,i_2)$ for the fragments; its elements are calculated according to the equation:

$$K_{AB}(i_1,i_2)=\frac{1}{\sqrt{\sum_k {O_{A,i_1}}^2(k)\sum_k {O_{B,i_2}}^2(k)}}\max_r\left(\sum_k O_{A,i_1}(k)O_{B,i_2}(k+r)\right)$$

The obtained correlation matrix shows similarity of the selected fragments. The maximal values of the matrix $K_{AB}(i_1,i_2)$ correspond to pairs of the most similar fragments. However, the correlation matrix does not indicate the selected fragments relative location, and does not take into account that all fragments have to be rotated by an equal angle. Moreover, not all fragments have its own pairs in the selected sets of the control fragments. So analysis of the obtained correlation matrix cannot lead to correct matching of the coresponding control fragments.

The proposed technique of control fragments matching uses an analysis of the correlation matrix and of the information on fragments relative location. It is based on the technique, proposed by *Ranade & Rosenfeld* [3.5] and modified by *J.K.Cheng* & *T.S. Huang* [3.6] and *J.Ton* & *A.K.Jain* [3.7].

This technique is iterative. At the first step, the correlation matrix is normalized to make the sum of each matrix raw equal to 1. So a matrix of original probability of fragments coincidence $P^0(i_1i_2)$ is obtained. The element of this matrix $P^0{}_{i_1i_2}$ indicates the probability of correspondence of the fragment i_1 from the image A to the fragment i_2 from the image B. During the next steps, this matrix is modified taking into account relative location of the fragments.

Each pair of fragments i_1 and i_2 'collects support' from other fragments towards its similarity. Let us suppose, that the fragment pair i_1 è l_2 from the A and B images is true. Then the fragment j_2 from the image B may be found for every fragment j_1 of the image A such that the distance $d_{i_1j_1}$ from i_1 to j_1 must be equal to the distance $d_{i_2j_2}$ from i_2 to j_2 . Then the fragment j_1 corresponds to a fragment j_2 . In such a case the fragment pair j_1 and j_2 give its support towards fragment pair i_1 and i_2 .

The probability of this fragment pair match $P^l{}_{i_1i_2}$. changes correspondingly.

$$P^{l+1}{}_{i_1i_2}=P^l{}_{i_1i_2}\cdot S^l{}_{i_1i_2}\ ,$$

where *l* is the iteration number, $S^l{}_{i_1i_2}$ - collected support for the pair from other pairs. The value $S^l(i_1,i_2;j_1,j_2)$ of the support, given by the fragments pair j_1 and j_2 towards the fragments i_1 and l_2 match ($0\le S^l(i_1,i_2;j_1,j_2)\le 1$) depends on the distance between the fragments and is calculated according to the equation:

$$S^l(i_1,i_2;j_1,j_2)=P^l{}_{j_1j_2}\cdot\min\left(\frac{d_{i_1j_1}}{d_{i_2j_2}},\frac{d_{i_2j_2}}{d_{i_1j_1}}\right),$$

where $d_{i_1j_1}$ and $d_{i_2j_2}$ are distances between the corresponding fragments.

The support, gathered by the i_1 and i_2 pair is assembled according to:

$$S^{l}_{i_1 i_2} = \frac{1}{n_1} \sum_{j_1=0,\, j_1 \neq i_1}^{n_1} \left\{ \max_{0 \le j_2 < n_2,\, j_2 \neq i_2} \left(S^{l}(i_1, i_2; j_1, j_2) \right) \right\}.$$

The matrix of the fragments match probability calculated at the current step is normalized to provide the sum of each matrix raw to be equal to 1.

The iterative probability matrix modification results in an increase of its elements corresponding to true fragment pairs. The probability of true fragment pairs match approaches to 1. In the ideal case after some iterations, the result matrix would be obtained with elements equal to one in they correspond to true pairs and with all other elements equal to zero. As the result, the true matched pairs of fragments from the images A and B would be obtained. Parameters for one original image transformation to co-registrate it with the other may be obtained by the consequent co-registration of these fragments.

The number of selected fragments from sets A and B in real conditions is different and the matrix is rectangular. Moreover, the selected fragment sets do not contain the same fragments. It complicates fragment matching. In such a case the matrix elements corresponding to impossible pairs get values near zero, and possible pairs obtain significant non-zero values. The true fragment pairs may be recognized by selecting maximal values in each probability matrix column.

The described algorithm matches fragment pairs using information on their relative location. It is possible to find true pairs even if the original probability matrix is uniform (i.e. there is no apriori information on similarity of fragments). However the iterative process is quite laborious and it is necessary to perform dozens steps to obtain a solution. The amount of calculations for each iteration depends on square of the number of fragments n_1. n_2. Computational time may be decreased by an initial probability matrix specification. In case of selection from images with a large number of fragments, which cannot be matched, it is difficult to find the correct solution and the technique may fail. Specification of the initial probability matrix makes it possible to find true control fragment pairs even under such conditions.

The process of fragment pairs matching may require a manual correction in a case if the algorithm cannot match fragments correctly. An operator may fix some true control fragment pairs. The corresponding probability must be set to be equal to one for it in the initial probability matrix. The rest of the elements in the corresponding raw of the matrix must be set equal to zero. Other fragment pairs would be matched automatically after it.

A.2.2 Example of control points selection

The proposed technique of control fragments selection was used on two test images. Two images of 320 x 320 pixels were used for this purpose. These images were the first and second channels of the multispectral image, received from the SPOT s/c. One of images was rotated relative to another by a small angle of ~5° and shifted for a distance of few pixels. This experiment was aimed to simulate the co-registration of two images in

various spectral bands after the a preliminary rough co-registration according to the ballistic information. One of the used test images is shown in Fig.3-10.

Fig.3-10. The first of the original test images - the first channel of the multispectral image, obtained from the SPOT s/c. A part of the whole image of 320 x 320 pixel was used for the experiment.

Both test images were convolved with the Laplassian mask in order to detect borders; images were thresholded after it. The threshold was 35 and 40 correspondingly. The obtained binary images are shown in Fig.3-11 and Fig.3-12. The images were splitted into fragments of 32 x 32 pixels. The splitting was performed with a 50% overlap. Then Hough transformation was performed for each fragment (the number of distinguishable directions was chosen to be equal to 36), uniformity vectors were calculated and the measure of crossing lines presence was evaluated. The values of the measure are listed in Table.3-1 and Table.3-2. 20 fragments with the highest values of the measure of crossing lines presence were selected among all fragments with the number of marked points greater than 20. The selected fragments are marked by square frames in Fig.3-10 and Fig.3-11.

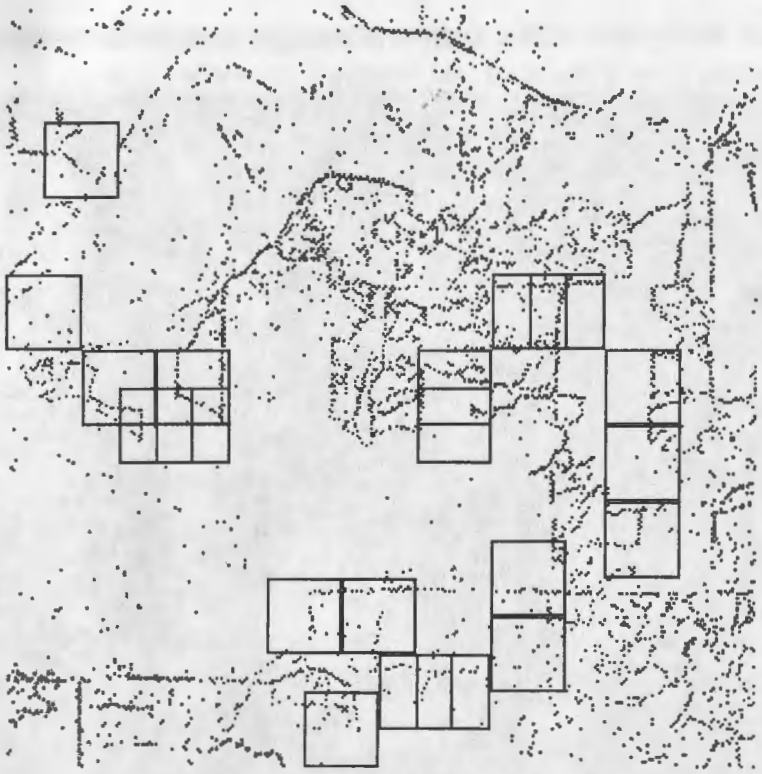

Fig.3-10. First of binary images after borders detection and thresholding. The selected fragments are marked by frames.

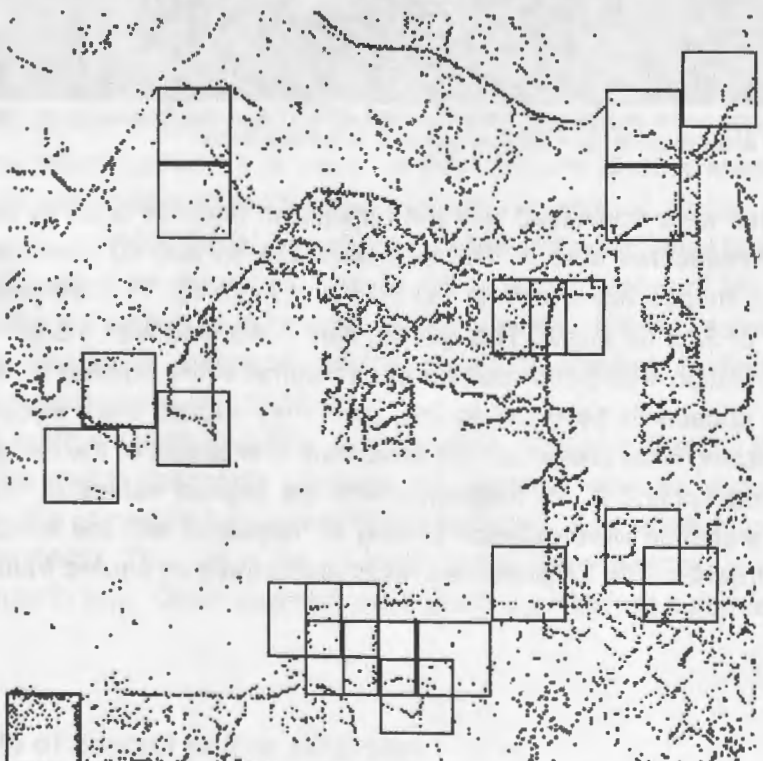

Fig.3-11. The second binary image. The original image is the second-channel image obtained from SPOT s/c and rotated by 5 degrees. The image was processed to detect borders and thresholded. The selected fragments are marked by frames.

Table.3-1. *Measures of crossing lines presence in fragments of the first test image. The selected fragments are marked.*

6.3	5.0	4.8	4.0	2.5	5.7	6.2	5.1	2.3	4.7	2.6	3.7	4.5	6.3	4.7	0.0	0.0	0.0	0.0
6.8	8.5	9.9	6.6	4.5	3.8	4.0	5.6	3.5	3.3	3.6	5.2	3.5	2.0	3.1	5.3	4.7	5.9	4.8
5.4	5.4	5.0	3.9	2.9	5.0	3.9	4.7	5.0	4.7	4.7	2.6	3.6	5.4	3.3	4.7	6.0	2.7	2.3
2.9	10.1	2.1	3.7	3.3	2.5	4.5	3.1	4.7	1.8	4.4	3.1	2.4	3.7	5.1	4.6	2.8	4.8	1.9
5.0	6.5	4.5	0.1	3.8	3.7	5.9	2.2	3.0	2.8	3.2	3.3	2.9	3.1	2.9	3.8	4.7	6.1	4.0
4.1	5.2	5.7	4.0	5.2	4.0	2.5	2.4	1.7	2.9	3.0	2.3	2.4	4.8	3.1	2.5	4.4	2.4	4.0
3.1	5.3	6.5	5.5	3.4	2.2	1.7	3.0	1.4	2.2	4.3	3.3	1.8	3.6	3.2	2.8	3.8	3.8	1.9
8.8	6.3	4.7	6.9	3.4	3.8	4.0	4.5	2.9	2.0	2.6	1.6	2.2	8.9	12.6	2.9	4.1	2.3	2.7
2.4	3.0	6.8	5.8	1.9	2.4	4.9	3.3	2.2	1.8	3.4	2.1	1.4	5.0	3.0	0.0	3.5	3.2	3.0
1.7	2.6	9.6	4.2	9.3	3.3	5.3	2.5	1.7	2.1	2.7	7.2	1.8	3.7	6.4	6.7	7.4	5.7	5.9
5.4	3.8	6.7	8.8	12.7	5.3	4.8	8.6	3.3	2.4	2.4	12.7	2.0	4.1	6.1	5.2	4.1	2.5	4.1
7.3	2.1	5.2	4.4	0.0	0.0	0.0	0.0	5.0	3.6	5.0	1.7	0.1	4.9	2.6	2.9	7.7	3.0	4.5
8.2	4.0	2.8	3.3	2.4	3.1	0.1	0.0	0.0	0.0	0.0	2.2	0.0	4.3	1.8	3.2	6.5	6.4	3.4
0.0	0.0	3.7	3.9	3.4	6.8	3.3	0.0	0.0	4.7	3.3	3.5	0.2	4.8	2.9	4.2	10.3	6.2	4.1
10.1	3.7	7.0	5.5	3.7	5.7	4.1	4.3	3.6	4.4	3.6	5.2	4.6	8.2	3.5	2.1	4.4	6.2	4.5
7.6	3.7	5.7	6.6	0.1	0.0	0.0	11.1	5.3	8.4	5.4	2.4	4.3	5.4	2.8	2.8	2.6	1.6	2.0
2.7	3.7	4.3	3.4	4.1	3.9	2.2	3.9	3.7	6.3	4.3	4.3	3.6	7.1	3.6	3.3	2.4	1.4	1.5
6.5	6.1	1.5	2.0	2.3	6.5	2.8	2.5	1.9	4.4	8.7	11.5	3.7	4.5	5.0	2.1	4.0	4.1	2.6
5.8	4.8	2.8	3.8	4.1	5.3	2.7	3.8	8.0	5.4	7.5	4.0	4.4	4.7	2.9	4.6	3.9	3.1	2.4

Table.3-2. *Measures of crossing lines presence in fragments of the first test image. The selected fragments are marked.*

5.0	3.1	4.9	9.2	5.5	4.8	3.3	3.4	4.6	2.2	2.8	2.6	1.9	3.7	3.3	0.0	0.0	0.0	4.0
6.3	7.8	5.3	5.4	5.7	2.3	4.8	5.0	6.0	8.5	4.7	2.0	1.5	1.5	2.6	6.9	4.0	0.0	7.0
6.4	6.8	3.1	6.0	10.9	4.1	3.2	5.9	3.5	4.6	3.1	3.0	3.2	2.6	2.6	4.7	7.1	6.8	2.6
5.8	5.4	2.6	6.4	5.2	4.4	5.9	2.2	2.4	4.3	2.7	2.3	3.0	5.5	3.5	4.3	4.7	4.0	2.1
6.3	4.7	3.4	4.8	6.8	3.0	6.5	2.9	1.8	3.3	4.6	3.8	3.4	4.6	3.2	4.1	7.4	2.6	2.8
3.6	4.8	3.7	4.7	5.3	5.1	2.3	3.6	2.2	2.1	2.1	3.0	2.3	3.1	2.5	2.7	6.0	2.6	4.2
2.9	6.0	3.5	3.2	5.1	1.6	2.0	2.2	1.8	2.3	2.6	3.7	1.9	2.8	3.7	2.4	3.5	2.7	3.9
5.0	3.7	4.0	2.0	3.0	3.0	2.1	4.4	1.8	1.0	3.3	1.8	2.0	8.7	11.2	5.4	2.3	2.0	2.0
3.1	5.1	3.7	2.1	2.1	1.9	8.8	3.2	1.5	1.6	0.0	1.7	2.7	1.3	2.8	0.9	3.3	1.3	2.8
2.2	3.1	7.5	4.3	3.7	2.5	6.6	4.0	1.7	0.0	2.1	3.0	1.8	2.9	3.9	2.7	6.0	4.0	2.5
4.2	2.5	4.2	2.8	11.5	3.3	16.0	2.5	2.6	4.0	3.6	3.2	1.7	3.3	2.8	4.4	3.0	2.7	2.3
5.5	7.2	6.7	4.3	4.5	4.3	5.9	10.0	4.3	3.9	3.7	4.5	8.7	2.6	2.0	3.8	4.0	2.0	3.0
6.5	4.1	3.2	3.7	0.0	0.0	0.0	0.0	0.0	0.0	0.0	0.0	5.5	3.3	2.4	3.0	5.7	1.7	1.7
0.0	0.0	3.3	2.8	2.8	5.4	6.7	0.0	0.0	0.0	0.0	0.0	0.0	2.6	2.5	4.4	11.3	3.7	2.7
5.0	4.7	7.5	2.7	3.4	5.9	5.0	2.9	3.2	3.4	2.8	3.9	5.4	7.6	4.0	2.8	3.2	7.2	3.2
5.5	7.3	5.7	7.2	3.3	3.3	5.5	7.8	9.4	3.7	3.8	5.3	5.1	4.1	2.1	2.6	2.7	2.4	1.7
7.6	2.2	4.4	8.0	3.3	3.3	3.9	4.0	7.8	14.8	6.6	7.1	5.2	4.4	2.9	3.6	2.3	1.7	2.1
1.4	3.9	2.5	2.1	3.8	3.2	1.9	2.3	3.5	6.7	6.9	4.9	6.1	3.8	4.6	3.2	3.6	1.9	2.6
7.2	4.3	3.1	2.4	4.5	4.5	3.3	3.5	4.0	6.8	3.1	5.0	6.2	4.0	2.7	6.0	2.4	2.3	1.8

The obtained uniformity vectors of the selected fragments were compared according to the described above technique. The calculated correlation matrix show the degree of

similarity of the selected fragments. The correlation matrix was normalized, and the initial matrix of fragments coincidence probabitity was obtained as shown in table.3-3.

Table.3-3. *Correlation matrix of fragments. Pairs of coincident fragments are marked.*

1 \ 2	1, 18	2, 4	2, 16	4, 4	4, 16	7, 13	7, 14	9, 2	10, 4	11, 1	13, 16	14, 13	14, 17	15, 7	15, 8	16, 8	16, 9	16, 11	17, 10	18, 0
[3,1]	0.08	0.08	0.08	0.08	0.02	0.00	0.01	0.03	0.04	0.09	0.04	0.02	0.02	0.08	0.07	0.07	0.06	0.09	0.04	0.00
[7,0]	0.09	0.12	0.04	0.11	0.01	0.00	0.01	0.02	0.02	0.13	0.02	0.01	0.01	0.07	0.05	0.03	0.09	0.13	0.05	0.00
[7,13]	0.07	0.08	0.05	0.08	0.03	0.01	0.03	0.04	0.04	0.09	0.04	0.04	0.03	0.07	0.05	0.04	0.06	0.09	0.04	0.02
[7,14]	0.07	0.08	0.05	0.07	0.04	0.01	0.02	0.06	0.05	0.08	0.05	0.04	0.04	0.06	0.05	0.04	0.06	0.08	0.04	0.01
[9,2]	0.08	0.08	0.07	0.08	0.02	0.00	0.01	0.03	0.03	0.09	0.04	0.02	0.02	0.08	0.07	0.06	0.06	0.09	0.05	0.00
[9,4]	0.07	0.08	0.05	0.07	0.04	0.01	0.02	0.06	0.05	0.08	0.05	0.04	0.04	0.06	0.05	0.04	0.06	0.08	0.04	0.01
[9,11]	0.07	0.08	0.05	0.08	0.04	0.01	0.03	0.04	0.04	0.09	0.04	0.04	0.03	0.07	0.05	0.04	0.06	0.09	0.04	0.02
[9,16]	0.07	0.08	0.06	0.07	0.04	0.01	0.02	0.05	0.06	0.08	0.06	0.03	0.04	0.06	0.05	0.04	0.06	0.08	0.04	0.01
[10,3]	0.08	0.12	0.03	0.11	0.01	0.00	0.01	0.02	0.02	0.14	0.02	0.01	0.01	0.06	0.04	0.02	0.13	0.13	0.04	0.00
[10,4]	0.08	0.12	0.03	0.11	0.01	0.00	0.01	0.02	0.02	0.14	0.02	0.01	0.01	0.07	0.04	0.02	0.12	0.13	0.04	0.00
[10,11]	0.08	0.12	0.04	0.11	0.01	0.00	0.01	0.02	0.02	0.14	0.02	0.01	0.01	0.07	0.05	0.03	0.10	0.13	0.04	0.00
[11,16]	0.08	0.08	0.08	0.08	0.02	0.00	0.01	0.03	0.03	0.09	0.04	0.02	0.02	0.08	0.07	0.06	0.06	0.09	0.05	0.00
[13,16]	0.07	0.08	0.06	0.08	0.03	0.01	0.01	0.05	0.05	0.09	0.06	0.03	0.03	0.07	0.05	0.05	0.06	0.08	0.04	0.01
[14,13]	0.07	0.08	0.08	0.08	0.02	0.00	0.01	0.04	0.04	0.09	0.05	0.02	0.02	0.07	0.06	0.06	0.06	0.09	0.04	0.01
[15,7]	0.08	0.12	0.03	0.11	0.01	0.00	0.01	0.02	0.02	0.15	0.02	0.01	0.01	0.06	0.04	0.02	0.12	0.13	0.04	0.00
[15,9]	0.08	0.09	0.07	0.08	0.02	0.00	0.01	0.03	0.03	0.09	0.04	0.02	0.02	0.08	0.08	0.06	0.06	0.09	0.05	0.00
[16,13]	0.09	0.12	0.04	0.12	0.01	0.00	0.01	0.02	0.02	0.12	0.02	0.01	0.01	0.08	0.05	0.03	0.08	0.12	0.05	0.00
[17,10]	0.10	0.11	0.04	0.12	0.01	0.00	0.01	0.02	0.02	0.11	0.02	0.01	0.01	0.08	0.06	0.03	0.08	0.11	0.06	0.00
[17,11]	0.08	0.12	0.03	0.11	0.01	0.00	0.01	0.02	0.02	0.14	0.02	0.01	0.01	0.07	0.05	0.02	0.12	0.13	0.04	0.00
[18,8]	0.09	0.09	0.06	0.09	0.01	0.00	0.01	0.02	0.02	0.09	0.03	0.01	0.01	0.10	0.08	0.05	0.07	0.09	0.06	0.00

Iterative process of probability matrix modification after 100 iterations was resulted in the final matrix of fragments coincidence probability as shown in Table.3-4.

Table.3-4. *The final probability matrix of selected fragments coincidence. The found true pairs of coincident fragments are marked.*

1 \ 2	1, 18	2, 4	2, 16	4, 4	4, 16	7, 13	7, 14	9, 2	10, 4	11, 1	13, 16	14, 13	14, 17	15, 7	15, 8	16, 8	16, 9	16, 11	17, 10	18, 0
[3,1]	0.00	1.00	0.00	0.00	0.00	0.00	0.00	0.00	0.00	0.00	0.00	0.00	0.00	0.00	0.00	0.00	0.00	0.00	0.00	0.00
[7,0]	0.00	0.16	0.00	0.84	0.00	0.00	0.00	0.00	0.00	0.00	0.00	0.00	0.00	0.00	0.00	0.00	0.00	0.00	0.00	0.00
[7,13]	0.00	0.00	0.00	0.00	0.00	1.00	0.00	0.00	0.00	0.00	0.00	0.00	0.00	0.00	0.00	0.00	0.00	0.00	0.00	0.00
[7,14]	0.00	0.00	0.00	0.00	0.00	0.00	1.00	0.00	0.00	0.00	0.00	0.00	0.00	0.00	0.00	0.00	0.00	0.00	0.00	0.00
[9,2]	0.00	0.00	0.00	0.00	0.00	0.00	0.00	0.99	0.00	0.01	0.00	0.00	0.00	0.00	0.00	0.00	0.00	0.00	0.00	0.00
[9,4]	0.00	0.00	0.00	0.00	0.00	0.00	0.00	0.82	0.18	0.00	0.00	0.00	0.00	0.00	0.00	0.00	0.00	0.00	0.00	0.00
[9,11]	0.00	0.00	0.00	0.00	0.00	0.59	0.41	0.00	0.00	0.00	0.00	0.00	0.00	0.00	0.00	0.00	0.00	0.00	0.00	0.00
[9,16]	0.00	0.00	0.00	0.00	0.00	0.00	0.00	0.00	0.00	0.00	0.12	0.00	0.88	0.00	0.00	0.00	0.00	0.00	0.00	0.00
[10,3]	0.00	0.00	0.00	0.00	0.00	0.00	0.00	0.25	0.12	0.63	0.00	0.00	0.00	0.00	0.00	0.00	0.00	0.00	0.00	0.00
[10,4]	0.00	0.00	0.00	0.00	0.00	0.00	0.00	0.00	1.00	0.00	0.00	0.00	0.00	0.00	0.00	0.00	0.00	0.00	0.00	0.00
[10,11]	0.00	0.00	0.00	0.00	0.00	0.48	0.51	0.00	0.00	0.00	0.00	0.01	0.00	0.00	0.00	0.00	0.00	0.00	0.00	0.00

[11,16]	0.00	0.00	0.00	0.00	0.00	0.00	0.00	0.00	0.00	0.00	0.79	0.00	0.21	0.00	0.00	0.00	0.00	0.00	0.00	0.00
[13,16]	0.00	0.00	0.00	0.00	0.00	0.00	0.00	0.00	0.00	0.00	1.00	0.00	0.00	0.00	0.00	0.00	0.00	0.00	0.00	0.00
[14,13]	0.00	0.00	0.00	0.00	0.00	0.00	0.00	0.00	0.00	0.00	0.00	1.00	0.00	0.00	0.00	0.00	0.00	0.00	0.00	0.00
[15,7]	0.00	0.00	0.00	0.00	0.00	0.00	0.00	0.00	0.00	0.00	0.00	0.00	0.00	1.00	0.00	0.00	0.00	0.00	0.00	0.00
[15,9]	0.00	0.00	0.00	0.00	0.00	0.00	0.00	0.00	0.00	0.00	0.00	0.00	0.00	0.24	0.73	0.03	0.00	0.00	0.00	0.00
[16,13]	0.00	0.00	0.00	0.00	0.00	0.00	0.00	0.00	0.00	0.00	0.00	0.00	0.00	0.00	0.00	0.00	0.00	1.00	0.00	0.00
[17,10]	0.00	0.00	0.00	0.00	0.00	0.00	0.00	0.00	0.00	0.00	0.00	0.00	0.00	0.00	0.00	0.44	0.16	0.00	0.40	0.00
[17,11]	0.00	0.00	0.00	0.00	0.00	0.00	0.00	0.00	0.00	0.00	0.00	0.00	0.00	0.00	0.00	0.00	0.62	0.00	0.37	0.00
[18,8]	0.00	0.00	0.00	0.00	0.00	0.00	0.00	0.00	0.00	0.00	0.00	0.00	0.00	0.03	0.00	0.12	0.06	0.00	0.78	0.00

The final probability matrix analysis resulted in selection of true fragment pairs. 9 matched pairs of coincident fragments were selected among 20 fragments of the first image and 20 fragments of the second image. The found fragment pairs are listed in Table.3-5.

Table.3-5. *The final table of the found fragment pairs.*

N	y_1	x_1	y_2	x_2	a	Dy	Dx	cpy_1	
1	7	13	7	13	0	0.2	0.1	128	
2	7	14	7	14	0	3.7	-2.6	128	
3	9	2	9	2	0	5.8	-3.6	160	
4	10	4	10	4	0	3.2	-4.0	176	
5	13	16	13	16	17	-4.1	-4.1	224	
6	14	13	14	13	0	1.3	-1.9	240	
7	15	7	15	7	35	2.7	-1.3	256	
8	15	9	15	8	35	0.5	20.6	256	
9	17	10	17	10	0	1.5	-2.4	288	176

The angle of rotation and the values of translation of fragments of the second image relative to corresponding fragments of the first image were evaluated at the final step. It was performed according to the described above technique with the use of uniformity vectors and Hough transformations of fragments.

The obtained angle of fragment rotation was 0 or 35, that correspond to the rotation angle of 0° or 5°. The fifth pair of fragments provide another angle of rotation 17 (90° - 5°). It may be explained by the fact, that the fragments include lines crossing at the angle of 90°.

The obtained values of fragment translations make it possible to evaluate coordinates of control points for estimation of the transformation matrix. Centers of the selected fragments are control points in the first (reference) image. In the second (matched) image, control points are shifted relative fragment centers by values, equal to relative shifts of corresponding fragments. The obtained coordinates of control points for the matched and the reference images are listed in Table.3-5. These coordinates may be used for estimation of the transformation matrix of the matched image to co-register it with the reference image.

A2.3 Conclusion

The technique to co-registrter images on the base of detection and comparison of control features in a form of intersections of linear elements was proposed as a result of the research. Such features are usually preserved in images in various spectral bands. It makes it possible to use the proposed technique for co-registrateion of images in different bands where traditional correlation techniques usually fail.

Rectilinear features may be easily identified, their orientation may be estimated with a high degree of accuracy. Rectilinear features detection is performed by the Hough transformation. It may be characterized by the property of high resistance to noise in the image.

Automatic control features selection on the both images makes it possible to use a large number of fragments, increasing the accuracy of subsequent co-registration.

Pair matching of the coincident control features of the reference and the target images is performed using fragments description and the information on their relative location. It makes it possible to find true pairs even in a case of small number of coincident fragments. An operator has to take part in the process in the worst case. He may fix one or more pairs of coincident fragments. The other pairs are matched automatically after it. The technique was tested on the simulated images.

Development of the proposed technique is not completed. The research has to be continued and completed by a series of experiments on co-registration of images of various natural regions, obtained in different spectral bands by various sensors in order to estimate the efficiency of the technique and recommend it for practical use.

Further research may be aimed first of all at using the proposed technique for co-registration of images with the sufficiently different resolution, at the co-registration accuracy estimation of images of various landscapes obtained by various sensors.

The question of fragment size optimization as function of image parameters seems to be interesting.

A specialized technique of border detection in images is to be developed, aimed at the enhanced linear sectors of border detection. It is important to improve the described control features matching technique to speed it up in the case when the number of fragments is large. Moreover, a development of the proposed matching technique is required to use the similarity of uniformity vectors besides information on their relative location during modification of the probability matrix by collection of support to a fragments pair.